DESIGN AND EVALUATION OF A DOSIMETRY SYSTEM TO VERIFY THE RADIOTHERAPY PROCEDURE FROM TREATMENT PLANNING TO TREATMENT DELIVERY

By

Mulape M. Kanduza

Submitted in fulfillment of the requirements for the degree of Master of Science (Medical Physics) in The department of Radiation Oncology, Faculty of Health Sciences, University of Pretoria, Pretoria.

March 2005

In dedication to my parents Esther and Ackson Kanduza.

Table of contents

ACKNOWLEDGEMENTS

"Potential is purpose unfulfilled"

Embarking on a masters must be one of the easiest decisions I have made. But to complete, it takes a whole lot more. This is how I feel as I complete my dissertation. This is by no means a full testimony of the insight I have gained in the medical physics field but a demonstration of a task bestowed upon me by regulation and more so as a means to accomplish something I can safely say I did.

I beg forgiveness of those I may not mention but have contributed in one way or another to the outcome of this project. In the same breadth I have to mention the few who made the most impact. Foremost, I thank God in whom I believe and have depended upon all my life for everything more especially in times when the roads ahead seemed bleak and having a spiritual father made me strive on.

To my father Prof. A.M. Kanduza, whose encouragement and persuasion led me to this point. Dad, you had always said the only asset you can give me is education this is my gift to you and To my mother, Mrs E. Kanduza, despite the odds, you inspired me to achieve and aim high. Mom, Dad I am proud to be your daughter, "ndibonga kosa sila". To my brothers and sisters, Nyasi, Chikalipo, Eunice, Matembo, Fungu and Esther realize that there is only so much anybody can give you in this world and it is up to you to make the best you can of it. To

my niece and nephew, Lesa and Wakhile, you still have your whole lives ahead of you, enjoy your childhood.

To my confidante, I appreciate a great deal your support and encouragement. Thank you.

To my mentor, Prof A.J. van Rensburg, you have instilled in me a passion for medical physics. I am deeply gratified that I had the privilege to be under your supervision. There can only be one of each one of us in this world and for me I have gained intellectually from you and know that there is more to life that one can gain. Thank you for your patience and advice. Baie Dankie.

To my colleague, Emma Mercer, thanks a million for your insight and measureless advice.

Special thanks to Mr. Henny Kruger, who skillfully constructed the phantom. The ladies in planning, especially Juanita, for preparing the plans. To the radiographers who helped me with all the CT- scanning, treatment delivery and also for giving me assistance whenever I asked. To all the staff in the Radiotherapy Oncology department of Pretoria Academic Hospital, thanks for accommodating me in your daily schedules of caring for patients.

I also extend my gratitude to the medical physics department at the Hillbrow radiation Oncology for allowing me to do my TLD readings at their center; and to the International Atomic Energy Agency for their financial support.

ABSTRACT

In the advent of more radiotherapy centers being set up across the African continent and the introduction of linear accelerators in addition to some of the already existing cobalt radiotherapy machines, it is apparent that verification of treatment delivery is necessary. Also, most audits in radiotherapy concentrated on radiation bean outputs and few exist that check the radiotherapy chain. A dosimetry system has been developed to address need to verify the radiotherapy chain. The aim of this study is to demonstrate dosimetric verification and the feasibility as well as cost effectiveness of manufacture of the dosimetry phantom using material locally available in the radiotherapy department. The phantom is designed and fabricated in the shape of a female pelvis bearing in mind the high incidence of cervical cancer more especially in Africa. It is designed with purpose of accommodating two dosimetric tools: thermoluminescence dosimeters (TLDs) and radiographic film. The delivery of external beam radiation therapy is evaluated for three different modalities by comparison of predicted and measured dose values.

Point dose values measured with TLDs were compared with predicted dose values and resulted in differences of ± 5 % were observed for uniform dose regions. Higher discrepancies (up to ± 28%) were observed for points in the penumbra (high dose gradient) of the radiation field. Isodose distribution were determined by radiographic film and compared with those predicted by the treatment planning system. Distance to agreement between predicted and measured isodoses was within ± 5mm.

The dosimetric verification methods were quantitative, qualitative and clinically practical. The fabrication of the phantom, dosimetric measurements and analysis demonstrate the feasibility and accuracy of the system for achieving treatment verification. Thus the system provides a means to verify the full radiotherapy chain from the point prior to and after treatment planning and through to treatment delivery.

1. INTRODUCTION

Radiotherapy has become an indispensable tool for the treatment of several cancers in the medical arena and, in its complexity, inherently brings in the requirement for accurate and precise diagnosis, treatment planning and treatment delivery. Radiation doses requires monitoring for the variety of treatment configurations one can come across[1,2]. A high level of accuracy needs to be maintained in order to ensure a very narrow margin of error. The probability of random and systematic errors cannot be neglected and needs to be accounted for lest treatment is compromised both in terms of loss of tumour control and/or damage to normal tissue [2,3,4]. In practical radiotherapy, a dose of ±5% to 10% can make a difference between an acceptable or adverse outcome. Acceptable limits of uncertainty have been documented in various reports. The ICRU recommends a ±5% acceptable limit of uncertainty[4]. Several other authors can be as stringent as suggesting a limit of ±3% which is still well within the ICRU recommended limit. Therefore it goes without saying that the requirement for quality assurance and quality control in radiotherapy needs to be encouraged. For optimization of treatment, it is important that the integrity of the entire planning process from the initial diagnosis through to treatment delivery be verified [2-5].

Uncertainties in dose are a result of one or a combination of several reasons. Systematic and random errors during the preparation of a treatment plan can be a source of flawed external radiotherapy treatment delivery[4]. Sources of error could stem from wrong calculation of dose distribution and monitor units and typically wrong prescriptions and or transcription of data from patient files into data files. Induced patient related

uncertainties could be the size, shape and composition of the patient in the area to be treated; unaccounted movement of the patient and internal organs as well as changes in the size and shape of the patient that may occur during treatment. These inherent problems can be taken into account as a component of dosimetric quality assurance. There are means one can employ to detect uncertainties introduced in radiotherapy treatment planning[5-7].

A number of authors have come up with ways in which one can assess radiation dose in radiotherapy. An independent confirmation of monitor units prescribed, dose distribution calculations and data transcription (recording and verification systems) can be performed via quality assurance programs. *In vivo* dosimetry systems and portal imaging devices are used to check treatment delivery[4-7]. Dosimetry procedures exist in most, if not all, radiotherapy departments. Dosimetry audits of the different techniques encompass dosimetry of radiation beams, treatment planning procedures and treatment delivery. Both on-site audits and mailed dosimetry programmes exist in parallel [8-10]. These audits provide a means of cross checking between what is done internally (on-site) and whether or not dosimetry done internally is actually within acceptable limits. To a large extent, these external audits are more concerned with radiation beam outputs and this creates reason to assess what is actually happening during treatment [10, 11].

Virtual simulation of patient set up and the final treatment plan are often done when the patient has left the radiotherapy department. Possible systematic errors may be introduced in the process of preparing a treatment plan. These may come from

inconsistencies of Digitally Reconstructed radiographs (DRR), inconsistencies of the beam dimensions with the virtual simulation software, laser misalignment in the CT, simulator and/or treatment rooms. Further, errors could be induced as a result of the user assigning incorrect beam parameters which may include gantry angles, collimator angle field size and patient dimensions [12].

CT simulation is an important radiation therapy tool. It ensures that the target volume is delineated accordingly. Actual checks involving patient set up parameters and final treatment plan need to be checked and verified for correspondence. Such external checks are by far the least of what may be required to ensure a thorough check and making sure that the target volume has been covered. Thus, it is important as it is that the entire radiotherapy chain be checked and reports on this type of verification of the entire planning process are scarce[12].

Radiation therapy aims at delivering pre-planned radiation dose within acceptable margins of uncertainty to selected sites in a patient's body. It is inevitable that some radiation dose will be delivered to tissues that are not the intended main target of treatment. However, different modalities of irradiation can be optimized so as to minimize the damage to such incidentally irradiated tissues. An audit of the external treatment planning and dose delivery can ensure this. By measuring the dose delivered by radiotherapy units and comparing these to what has been calculated be the treatment planning system (TPS) it is possible to verify treatment by measurements in phantoms [13, 14].

Dosimetry is an integral part in any radiotherapy department. It plays a major role in implementing proper and careful radiotherapy treatment of patients. It is a necessary tool for calibration and monitoring of the amount of dose delivered by a radiation therapy unit. Dosimetry involves the measuring of absorbed dose in a medium or a measure of the biological effects produced by ionising radiation. Dosimetric procedures may include[12].

(i) Thermo luminescence dosimetry

(ii) Film dosimetry

(iii) Ionisation dosimetry

(iv) Calorimetric dosimetry

(v) Chemical and gel dosimetry

(vi) Semiconductors (diodes)

The (i) to (iii) are of paramount interest in this study and will therefore be discussed in detail. The basic mode of operation is that radiation will alter a certain property of the dosimetry tool in question and this can then be translated into absorbed by established calculation methods and/or further analysis methods depending on what is the most appropriate evaluation criteria used.

Ionisation chambers are mostly used to determine absolute dose at a point. These are normally calibrated by the National Institute of Standards and Technology (NIST) or any NIST accredited laboratory. Calibration factors are then used to in the calculation methods of the absorbed dose at the point where the chamber had been placed in a therapy beam. Energy absorbed in a medium in which an ionisation chamber is embedded

can be derived from the energy absorbed in the ionisation chamber[2, 3]. TLDs, on the other hand, absorb energy when exposed to radiation. The stored energy is released as light when heated. The TLD response is characteristic of the radiation delivered and is proportional to the light produced. Thus, it is possible to calibrate the TLD before use and in this way be able to determine an unknown dose for an amount of light given off[3]. In film dosimetry, an image is produced when the film is irradiated. The darkening of the film corresponds to the absorbed radiation and this can be determined by densitometer scanning device[15].

Various protocols have been developed to ensure that continued and precise dosimetry checks are carried out in the different institutions that run radiotherapy programs[1]. These protocols cater for the calibration of both high- and low-energy photon and electron beams. These may include: the International Atomic Energy Agency (IAEA TRS 398), the American Association of Physicists in Medicine (AAPM TG-51, TG-21), the Institute of Physical Sciences in Medicine (IPSM) and the Institute of Physics in Engineering, Medicine and Biology (IPEMB)[16,17]. The continued development of dosimetry and calibration guidelines has enhanced the precision and accuracy in which dose measurements are performed and thereby optimising radiotherapy procedures[3,4,17]. Calibration of clinical photon and electron beams is necessary and needs to be monitored continuously. Developments in calibration methods have given rise to new dosimetric practices for high-energy clinical photon and electron beams. Most recent published protocol for clinical reference dosimetry have recommended absorbed dose to water

calibration for ionisation chambers. These provide a reference output calibration of radiation beams[17,18].

Regular quality control (QC) becomes necessary for any radiotherapy department. QC can be performed daily, monthly and annually for the verification of beam energy quality, output check, gantry and collimator rotation, correspondence between light and treatment field, verification of field flatness and field symmetry[5]. These are among the most common QC test performed on radiotherapy units (e.g. linear accelerators, cobalt- 60). The QC tests are commonly performed using film, TLD, ionisation chamber or a diode system. Regular patient dose monitoring is also an essential part of the quality assurance (QC) programmes. Treatment delivery in radiotherapy involves following certain precautionary criteria for proper execution. Treatment planning is therefore important for the prescription and calculation of dose, imaging for localisation of tumours and patient position. Computer programs are used in radiotherapy to calculate dose distributions in patients, treatment simulation conditions and data input for treatment planning [17,18].

Prior to treatment delivery, there are a number of problems that may be experienced in whole process. Patient positioning can be difficult and needs careful planning. Patients exhibit involuntary motion, changes in weight, and irregular contours and this can affect treatment planning let alone treatment delivery accuracy. More so is the reproducibility of the treatment set-up that ought to be maintained throughout the whole treatment chain. Normally one will find that as part of the treatment planning, markers will be used on the patient's skin surface as a means of ensuring reproducible positioning simulation to

treatment delivery. Patient dose calculations based on the initial localization procedures and proposed plan for treatment will have to be precise and accurate within limits[19].

Thus, precision is necessary in radiotherapy for effective treatment in terms of delivering an accurate dose and accurately covering the planned target volume (PTV). Difficulties may be experienced in defining and localizing the target volume with respect to external marks and precisely repositioning and immobilizing the patient can lead to poor optimisation of treatment delivery. Computed Tomography (CT) can assist in this aspect as it provides information on delineation of the target volume and the surrounding anatomical structures in relation to the external contour and also compositional density in the form of CT numbers. These CT images can be obtained under treatment conditions and thereby ease the treatment planning process[18].

Phantoms are by far the most appropriate way in which one can assess dosimetrical data. Phantoms can be designed in a variety of ways that lend themselves to specific treatment modalities and to a particular treatment site in relation to the human body. These may be used in order to evaluate the radiotherapy treatment chain. Phantoms may be used for imaging during the planning process on a simulator and/or CT scanner as well as being used for radiotherapy treatment delivery verification. They can also provide for dosimetric measurements at exact positions and depths and thereby make available information about beam parameters to be used in treatment planning [12, 18].

Many variations of phantoms have been developed that cater for different aspects. Some are suited for auditing treatment beams (photons or electrons); some for auditing specific parts of the radiotherapy treatment chain and yet some for specific treatment modalities.

The aim of this study is to design and demonstrate the principle behind a dosimetry procedure using a phantom to evaluate the accuracy and consistency of treatment delivery. An audit of the range of processes involved in the management of radiation therapy is desired. An assessment criteria based on the various dosimetric methods and tools is applied. A qualitative and quantitative account is provided as evidence.

2. THEORETICAL OVERVIEW

Radiation therapy is the treatment of neoplastic diseases, either begnine or malignant, with ionising radiation. The radiation can either be electromagnetic (x-rays, γ-rays) or corpuscular (electrons, protons, neutrons, alpha particles, mesons, heavy ions etc.). The radiation absorption effect is produced by the energy absorbed in living tissues through the process of ionisation and excitation of atoms as well as molecular constituents of the tissue. The radiation dose is the amount of energy absorbed by the tissue when a beam goes through the tissue [19]. As the photon beam (x-rays) impinges on the tissue, three outcomes are possible. These are that

(i) The photon may be absorbed by transfer of all its energy to the medium (tissue) by one or more interactions; or

(ii) The photon may be deflected and scattered in a different direction during an interaction (scattered radiation); or

(iii) The photon may be transmitted without interaction (primary radiation).

As a beam of photons passes through a medium, such as a patient's soft tissues, bone or any other structures in the body, various interactions will take place. These interactions tend to be competing processes. The relative dominance of each interaction depends on two major factors, which are (i) The photon energy, and (ii) the atomic composition of the medium[25]. Normally, because of the electrons short range, energy will be dissipated locally and the absorbed radiation becomes the cause of radiation effects or damage. On the other hand if a photon enters and leaves the medium without interacting then no radiation dose is delivered. Therefore, depending the photon energy and composition of

medium, the five major modes of interaction of photons with matter are: (i) Coherent Thompson Scattering, (ii) Photoelectric absorption, (iii) Compton Scattering, (iv) Pair Production, and (v) Photonuclear reaction or Photodisintegration. These interactions are mutually competing processes at all energies and their predominance and importance varies with increasing photon energies. At low energies (< 40kV) only (i) is important. At energies commonly used in radiotherapy (> 1MeV) (ii), (iii) and (iv) become important. At very high energies (> 20Mev) (v) plays the major role of interaction[25-22].

2.1 BEAM ATTENUATION

When a photon beam traverses through a medium, there is a diminishing effect on the photon flux (i.e. number of photons available for interaction). A fewer number of photons will emerge once the beam has traversed the medium and this is attributed to the fact that some of the photons will interact within the medium and are either absorbed or scattered [25-22]. A measurement of the attenuation of a photon beam can be done under narrow beam of broad beam geometry conditions. For narrow beam geometry the measurement is done at a location far from scatter whereas the broad beam geometry is done near scattering conditions. The loss in photon flux (attenuation) is directly proportional to the intensity of incident photons I and the thickness of the medium dx. Mathematically, this can be presented as

$$dI_x = -\mu I_0 \, dx \qquad (1)$$

Where μ is proportionality constant called the attenuation coefficient [21]. The negative sign indicates a reduction in the number of photons as the medium (absorber) thickness

increases. Since x is in units of length then μ becomes the linear attenuation coefficient and has units of the reciprocal of length (cm^{-1}). I_0 is the intensity of incident photons.

Equation (1) holds true if dI and dx are infinitesimally small. To find the photon flux, integration over a thickness x for reduction of I_0 *to* I_x

$$\int \frac{dI}{I} = -\mu \int dx \qquad (2)$$

Solving (2) yields

$$I_x = Io\, e^{-\mu x} \qquad (3)$$

This gives the exponentially attenuation of the beam under narrow beam geometry.

In the logarithmic form ln (I/I_0) decreases linearly with increasing thickness of attenuator [25-23].

The thickness of the medium can be expressed in terms of mass and yields the mass attenuation coefficient given as the linear attenuation divided by the density of the material (μ/ρ) with units $cm^2\ g^{-1}$. The mass attenuation coefficient is a better index for attenuation because it removes the role of density as compared to the linear attenuation coefficient, which may vary if the density of the medium changes. Furthermore, the attenuation capacity of a medium can also be given in terms of the atomic attenuation coefficient (μ_{atom}) and the electronic attenuation coefficient ($\mu_{electron}$) [25-23]. These can be expressed as:

$$\mu_{atom} = \frac{\mu A}{\rho N_A} cm^2 atom^{-1} \qquad (4)$$

and

$$\mu_{eleectron} = \frac{\mu_{atom}}{Z} = \frac{\mu A}{\rho N_{AV} Z} cm^2 electron^{-1} \quad (5)$$

Where A is the atomic mass and N_{AV} is Avogadro's number.

Each of the five processes by which photons interact with matter can be represented by its own attenuation coefficient. The total attenuation coefficient is the sum of the individual coefficients for theses processes given as [21]

$$\frac{\mu}{\rho} = \frac{\sigma_{coh}}{\rho} + \frac{\tau}{\rho} + \frac{\sigma_c}{\rho} + \frac{\pi}{\rho} \quad (6)$$

Where σ_{coh} , τ, σ_c , and π are the attenuation coefficients for Coherent Thompson scattering, Photoelectric absorption, Compton effect and Pair Production respectively.

2.2 PHOTON INTERACTIONS WITH MATTER

2.2.1 Coherent Thompson Scattering

This interaction occurs at very low photon energies. The interaction can be with a single electron or with multiple electrons. The electromagnetic field of the incoming photon induces an oscillation of the atomic electron as it passes near the atom. The incident photon will transfer its energy to the electron and will result in a deflection of the incident photon since the photon energy is not large enough to free the electron. The incident photon is scattered at small angles. The oscillating bound electron becomes a source of electromagnetic emission and it will reradiate the energy at the same frequency and energy as the incident photon. Coherent Scattering is most probable in materials with a high atomic number and with photons of relatively low energy. It is fairly negligible at

high-energy photons (megavoltage) and hence can be ignored at radiotherapy energy levels [20-25].

2.2.2 Photoelectric Absorption

This involves the total transfer of the energy of the incident photon to an inner electron of an atom of the medium exposed to radiation. In the photoelectric process, a photon of energy $E_\nu = h\nu$ collides with an atom and ejects on the bound electrons from the K, L, M, or N shells. The ejected electron is called a photoelectron and emerges with kinetic energy $E_k = h\nu - E_b$ where E_b is the binding energy of the photoelectron. For low-energy photons, photoelectrons are ejected at right angles and as the incident photon energy increases the photoelectron is ejected in a more forward direction. A vacancy is created by the ejected electron and this leaves the atom in an excited state[20,22]. Unless the energy $E_{\nu,}$ of the incident photon is sufficiently large ($E_\nu > E_{K,\ L,\ M\ or\ N}$, where $E_{K,\ L,\ M\ or\ N}$ are the binding energies of the electrons in the K, L, M and N shells) no interaction will occur [20-25].

Photoelectric attenuation depends on photon energy and on the atomic number (Z) of the material. The probability that it will undergo a photoelectric interaction decreases as $(1/E_\upsilon)^3$ of the photon energy. The probability of photoelectric attenuation varies as Z^3. The higher the atomic number of a material the higher the chances of the photoelectric effect to occur. There is a high probability of occurrence when low energy photons interact with high atomic number materials provided the photons have enough energy to overcome the binding energy of electrons in their shells[19,21].

In diagnostic applications low energy photons (< 40 kV) are of no importance because they are absorbed immediately due to their short range. However, the difference in the atomic numbers of various tissues amplifies the differences in x-ray absorption because of the high dependence of the photoelectric effect on the atomic number. Thus the Z^3 dependence of the photoelectric effect is exploited for contrast. The selective interaction of photons by photoelectric interactions in media with different atomic numbers and different physical densities renders low-energy x-rays useful for image formation. For tissues like bone as compared to muscle, fat and soft tissue, ideal contrast is observed for radiographs taken between 60-100 kV. Production of excellent quality images with good contrast is due to the fact that some tissues absorb more x-rays than other tissues [19,22-25]. Contrast is greatest when the difference in absorption between adjacent tissues is large. From the point of view of the film quality, photoelectric absorption is desirable because no scatter is produced. From the point of view of the patient, more radiation dose is received from photoelectric reactions more than any other type of interaction. The patient absorbs all the energy of the incident photon, which is more desirable in therapy [23].

2.2.3 Compton Scattering

Photons with energy between 30kV and 30MV can undergo interaction with outer-shell electrons that not only scatters the photon but also reduces its energy and ionises the atom [19, 20, 21]. An incident photon with relatively high energy strikes a free outer electron and ejects it from its orbit thereby ionising the atom. Part of the photon energy is transferred to a loosely bound or 'free' electron in the medium. The photon continues in an altered

path with decreased energy as scatter radiation. The electron is set into motion with a kinetic energy equal to the energy transferred by the incident photon less the binding energy that must be overcome in ejecting the electron from its orbit. An ion pair is produced; a positive atom and a negative electron (the recoil electron). Both the scattered photon and secondary electron may have sufficient energy to undergo more ionising interactions before losing all their energy. Ultimately, the scattered photon will be absorbed by photoelectric absorption [19,21].

An electron is termed free if the binding energy is less than that of the incident photon. The probability of occurrence of Compton scattering directly depends on the electron density (electrons per gram) of the absorbing medium. This is so because a medium with a higher electron density provides a higher concentration of electrons with which the incident photons can interact. The probability of Compton interaction decreases as the photon energy increases and is independent of the atomic number of the target medium[19].

Compton scattering occurs with all the diagnostics range x-rays. Its importance is two fold. In a positive sense, Compton scattering provides some contrast between air, bone and soft tissue through the differences in the linear attenuations which will create the difference in optical densities in the x-ray image produced. Image contrast is a reflection of the transmission variations of photons through the patient. In a negative sense, Compton scattered photons travel in all directions and contribute to film fog, which result in poor quality radiographs [21,25].

2.2.4 Pair Production

An incident photon with threshold energy (hν) enough for it to escape interaction with the electron cloud of an atom and will head towards the nucleus where it will be subjected to the strong electromagnetic field of the nucleus. The interaction between the photon and the nuclear electrostatic forces causes the photon to lose all its energy and in the process creating a pair of electrons; a positively charged positron and negatively charged electron. Two electrons are created, each of rest mass energy of 0.51 MeV.

The threshold energy of the incident photon is 1.02 MeV. A photon with energy less than 1.02 MeV cannot under go pair production. Probability of occurrence increases with increase in energy. Any of the excess photon energy (hν) is distributed equally between the two electrons as kinetic energy. The total kinetic energy available for the electron–positron pair is (hν - 1.02) MeV [25-21,25].

Since pair production results from interaction of the photon with the electromagnetic field of the nucleus, the probability of occurrence increases rapidly with atomic number. The mass attenuation coefficient for pair production varies almost linearly with the atomic number and increases gradually with the energy of the incident photon beyond the threshold energy. Because pair production occurs at megavoltage energies, which are outside of the diagnostic range, this interaction becomes unimportant in diagnostic radiology [19-25].

2.2.5 Photodisintegration

High enough photon energies can interact directly with the nucleus electromagnetic field and eject a nuclear particle when absorbed by a nucleus. When this happens, the nucleus is raised to an excited state and instantaneously emits a nucleon or other nuclear fragment [20,26]. The ejected fragment may either be a α-particle or a cluster of particles. Photon energies sufficient to overcome the nuclear binding energies range from 7-15 MeV. Photodisintegration rarely occurs in tissue but can occur in the shielding materials used around high-energy accelerators[22-25].

The relative importance of photoelectric, Compton and pair production are depicted in figure 1 below [21].

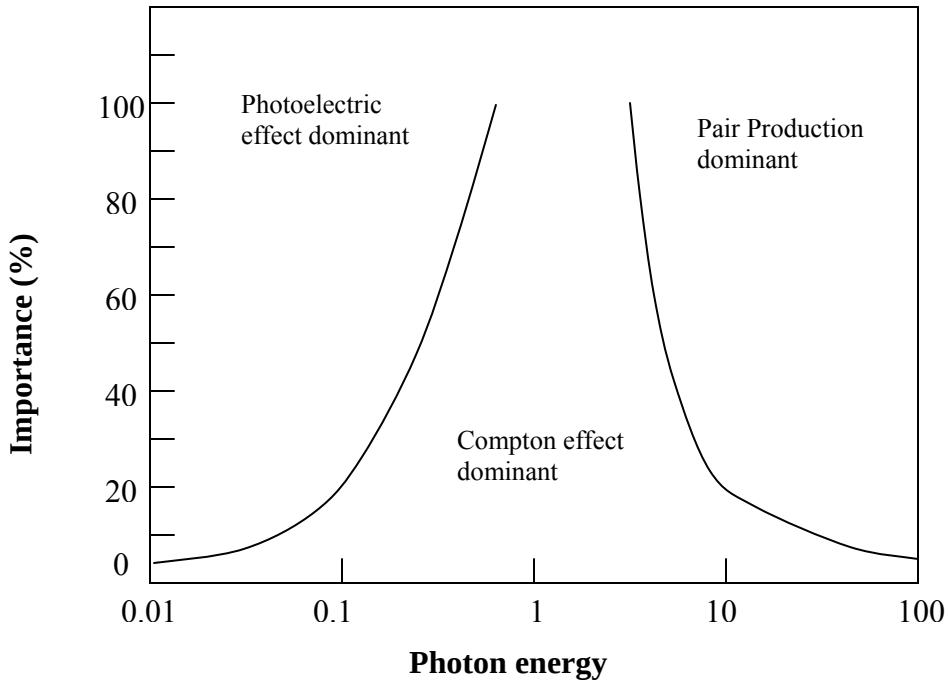

Figure 1 Relative importance of the three principles of interactions of photons with matter[25].

2.3 INSTRUMENTS FOR RADIATION DETECTION

Radiation can be detected by measuring the amount of effect produced by its interaction with matter. The radiation-induced effect on a radiation detector produces a signal that can be interpreted to give a radiation quantity [25]. Three methods will be considere due to their relevance in this study.

2.3.1 Ionisation detectors.

A thimble chamber is the most commonly used ionisation chamber. Principle of operation is based on the ionisation properties of air by radiation. The Ionisation chamber detects radiation by measuring the amount of charge liberated by the interaction of the radiation with suitable gases. The simplest form of chamber consists of two conducting electrodes in a gas filled thimble chamber. An electric field is maintained between the positive anode and negative cathode. Ionising radiation penetrates the chamber and liberates electrons form the gas atoms creating positively charged ions. The anode and the cathode collect ions and an electric field is created. The ion chamber signal is a current pulse, which flows as a result of the ionisation process [20-23].

Ionisation chambers are commercially available and a usually connected to an electrometer of high sensitivity for measurement of charge produced by radiation. The electrometer has a built in power supply to provide the necessary polarizing voltage to the ion chamber detector. When low voltage is applied to the detector, the ions are not collected quickly, and some may recombine prior to collection. The detectors response to a given amount of radiation will increase with increase in the applied voltage until a point

of saturation. It is at this point that all the ions are collected without any loss in recombination. Ionisation chambers used in practice operate at 150 –300 V [25,20].

2.3.2 Film Dosimetry

Radiographic film consists of a transparent film base (cellulose acetate) coated with an emulsion containing very small crystals of photosensitive silver halide (mostly silver bromide). When film is exposed to ionising radiation or visible light, a chemical change takes place within the exposed crystals to form a latent image. When the film is developed, the crystals that have been exposed to the radiation are reduced to small grains of metallic silver [25,20,25]. The developing solution makes use of the latent energy of the crystals and reduces the silver halide to pure silver. The film is then treated with a chemical that fixes the silver to the film base and clears off the silver halide. The metallic silver is not affected by the fixing solution and this darkens the film. Places where the film received a high dosage, the silver concentration will be high and the film will be darker as compared to places where a low dosage was received. In this way the film will give an image of the radiation absorption pattern [25,20].

The degree of darkness of the film is given in terms of optical density. This can be determined quantitatively by a densitometer. The densitometry has a light source that moves in line with a light-sensing detector (photocell). The intensity of the light that is transmitted through the film is quantified as the optical density *OD*, defined as

$$OD = \log \frac{D_0}{D_t} \qquad 7$$

Where D_0 is the amount of light measured without film and D_t is the amount of light transmitted through the film [20].

In dosimetry, the quantity of interest is the net optical density, which is a measure of difference between the unexposed processed films from the measured optical density.

Figure 2 below shows the net optical density as function of exposure (dose). This is called the sensitometric or H-D curve.

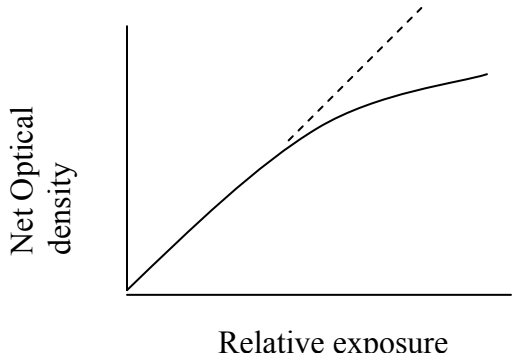

Figure 2 Sensitometric curve for film.

Sensitometric curves are used in film dosimetry for calibration purposes. The film linearity is important for dosimetry to ensure that the film is exposed to a dose within the linear region [20]. . Once exposed, the optical density is correlated to the dose by using depth dependence sensitometric curves. This gives percentage depth dose curves [20,26].

Film is not reliable for purposes of absolute dosimetry because of the variations in the crystal size, developing time, developer concentration, temperature and humidity[19].

Further, the silver in the film absorbs radiation below 150 keV mainly via the photoelectric effect. Because the photoelectric effect depends on the cube of the atomic number, the scatter produced strongly affects the film and the correlation between optical density and dose becomes strained. However, film is useful for checking radiation field, light field coincidence, field flatness and symmetry. Film is also used to measure isodose curves within acceptable accuracies of ±3 % [8,].

It is necessary to calibrate film when it is used as a dosimeter. In this case, the film is exposed to a radiation of known dose. Conditions of irradiating the film for calibration should closely match the conditions under which the beam was calibrated. The film is sandwiched between tissue-equivalent material of a thickness sufficient enough to provide secondary build up of electrons. Difference in irradiation times will match different dosages or exposures and correlated to a certain OD. The film can be characterised in terms of the variation of the film density with exposure [22].

The density is proportional for low exposures and low densities until it reaches a maximum, which indicates the point at which all the crystal grains have been developed. The film saturates at this point. Characteristic curves for any particular film should be known if the film is to be used as a dosimeter. Ideally, the exposure range should lie within the linear response region. Some films have low sensitivity and a wide range and some others may saturate quickly. A measure of the film sensitivity will depend on how fast a film will darken after exposure [12].

2.3.3 THERMO LUMINISCENCE DOSIMETERS (TLD).

The production of thermo luminescence in a material by exposure to ionisation radiation can be viewed in two stages:

(i) ionisation and electron trapping, and

(ii) Electron and hole recombination with photon emission.

Figure 3 shows a schematic representation of the thermo luminescence process [20].

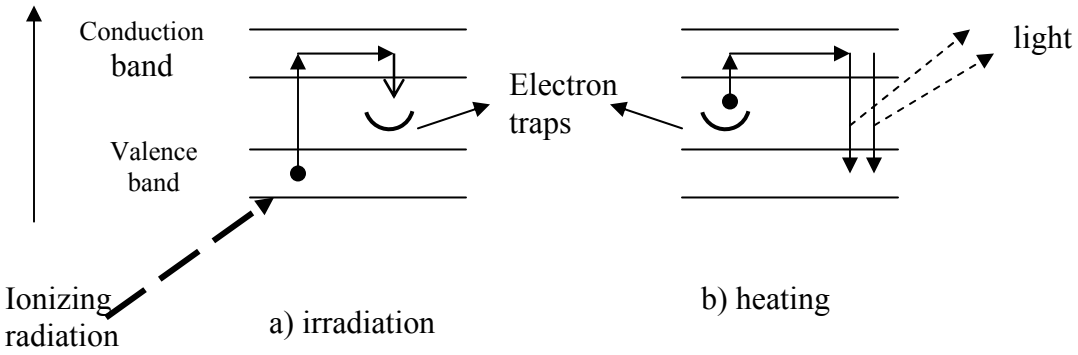

Figure 3 Thermo luminescence process [21].

Crystalline material exhibit thermoluminescence properties due to lattice defects. Ionisation radiation is absorbed in the material and free electrons are produced. Radiation may provide sufficient energy to raise the electrons from the valence band into the conduction band. The production of free electrons is associated with the production of free holes, which may migrate via the valence band and may be trapped. The vacancy created in the valence band is termed a positive hole. The electrons are free to move through the crystal and can get trapped if trapping levels exist in the forbidden energy gap between the valence and conduction bands. The holes are thermally unstable and may decay rapidly at normal room temperature [20,25].

The trapped electrons remain in their traps until they are thermally activated to escape. Is the temperature of the crystalline material is raised; the trapped electrons may acquire sufficient thermal energy and be released[25].

The absorbed energy due to radiation is stored in the crystal lattice and some of this energy is recovered as visible light when heated [20]. The heat acts as an agent to shake off the excited electrons trapped in any metastable energy state in the solid crystal. The electrons occupy discrete energy levels in the crystal. The electron traps are created in the crystal by the addition of impurities and interactions between atoms in the crystal. These traps exist in the forbidden energy gap[19-20].

The Glow Curve

The thermo luminescence signal is measured in a TLD reader because it is a weak signal. The TLD reader consists of a dark enclosure with a heating pad, a photomultiplier light sensor coupled to an amplifier, a meter for reading the integrated signal and a circuit for heating the sample. The intensity of the light emission with an increase in temperature will give a glow curve that has one or more peaks. These peaks (signal) are related to the absorbed dose D. The glow curve (figure 4) is a function of the thermo luminescence verses time. As the temperature of the TL material exposed to radiation is increased, the probability of releasing the trapped electrons increases. The glow curve consists of a number of peaks that correspond to traps at various energy levels[12,25].

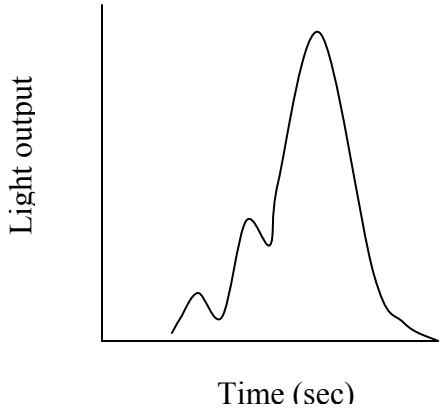

Figure 4 Typical glow curve for LiF showing relative output as a function of heating time [23].

TLD material is affected by previous thermal and radiation history. Before the TLD is used to measure an unknown dose, a known dose is used to establish a basis between the known and unknown dose signals. The dose-response correlation is established by use of the same quality of radiation as that in which the unknown dose is to be measured. This is done for calibration purposes. Dosimeters that have been used previously must be adequately annealed in order to remove any residual thermoluminescence memory[26].

Supralinearity and Sensitisation

TLDs respond linearly to dose up to a certain dose level beyond which the response becomes supralinear; i.e. it gives off a signal that increases more rapidly. Figure 5 below shows this response[23].

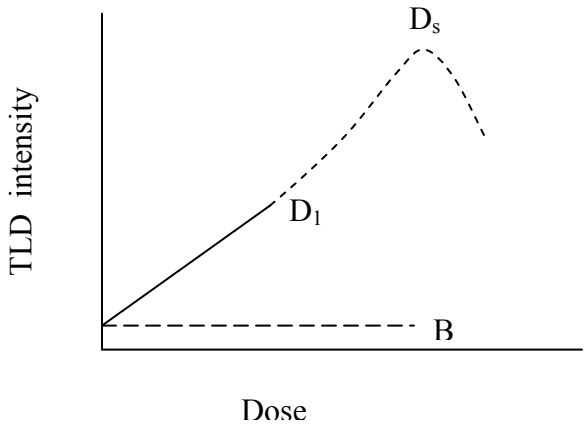

Figure 5 Typical TLD response versus dose curve.

The TL response per unit absorbed dose response is an important characteristic of a thermoluminescence material. At relatively low absorbed dose values the response is linear and is given by

$$TL = fD + B \tag{8}$$

where TL is the thermoluminescence signal (peak height or integrated signal) for an absorbed dose D, f is the TL emitted per unit absorbed dose, and B is the background signal from an unirradiated TLD[25].

Above dose D_1 in figure 5 above, the response of the TL is supralinear then saturating at D_s then falling off rapidly. An absorbed dose of approximately 25% less than D_s is generally taken to be practical upper absorbed dose limit [25]. The spontaneous emission of light is known as fading. The low temperature peaks, attributed to the release of electrons in the low lying traps, exhibit high fading of stored signal even at normal ambient temperature. These peaks have short half-lives. Thus to eliminate the glow from

these low traps, the TLDs can be read after hours or the TLD reader can be set to ignore the signal during the initial stage of the heating cycle (80-100^{0}C) [26].

In radiotherapy, TLDs can be used for intra-cavity exposure measurements. Radiotherapy treatment field geometrical set-ups, depth dose and transverse dose can be measured in phantoms. Other useful purposes of TLDs in radiotherapy are checking of machine outputs, beam uniformity checks and measurement of absorbed doses in phantoms. TL dosimeters give high precision, rapid retrieval of information, good environmental stability, good water and tissue equivalence and a wide range of sensitivities. Since TL dosimeters are small in size, they provide good spatial resolution, which is particularly useful in radiotherapy[26,27].

2.4 PHANTOM ABSORBED DOSE MEASUREMENTS

In radiotherapy, specification of absorbed dose distribution within the radiation beam can be measured in a phantom for calculating dose prescribed to the target volume[28]. Specification involves the use of published depth dose data and an isodose chart for the specified beam quality. Absorbed dose distribution in phantoms depends the beam dimensions and geometry, source-to-surface distance (SSD) or source-to-axis distance (SAD), as well as radiation quality and bam collimators. Thus, the ICRU[4] recommends the use of isodose charts exactly specified for a particular radiotherapy unit. The easiest method of measurements consists of (i) measuring depth dose distribution along the central axis of the beam in a phantom, and (ii) choosing one particular phantom depth at which measurements of the radiation absorbed dose profile are done[26-30].

2.5 TREATMENT PLANNING

Different kinds of radiotherapy machines are capable of producing beams of various qualities. Quality refers to type of radiation, the energy, and absorption and penetration capabilities. Penetration characteristics of any beam should be evaluated experimentally so as to facility controlled delivery of a radiation dose to a patient. There are a number of physical quantities used to define a radiation beam to aid in their clinical use[31]. Experimentally measured values of these quantities are useful for monitoring the day-to-day treatment of dose delivery in a patient. These parameters are also used to make comparison of beams for different qualities so as to select the most suitable for clinical use. For example, Tissue Air Ratio (TAR), Tissue Maximum Ration (TMR), Percentage Depth Dose (PDD) to mention a few [19,].

In order to ensure that a patient receives the correct dose, the patient needs to be properly positioned with respect to the radiation source. The parameters that specify the treatment geometry are: (i) the geometric centre of the beam or the central axis of the beam, (ii) the source-to-skin distance (SSD), (iii) the treatment depth d, and (iv) the cross-section of the beam or field size [19].

The SSD and the depth d give the distance of the source to a point at depth d called the source-to-axis distance (SAD). Any two of the three variables (SSD, SAD, and d) can define the third. This means that the SSD or SAD can be selected in advance for a specific treatment depth. Set-ups for isocentric machines are conveniently done at a pre-

selected SAD. For non isocentric machines, a pre-selected SSD is preferable. These are termed the fixed-SAD and fixed-SSD techniques respectively [17-21].

Radiation beam cross-sections do not have a sharp edge but have a penumbra. Most modern machines have rectangular shaped cross-sections. The beam dimensions can be specified at any depth or distance from the source[31].

2.6 DOSIMETRY OF RADIATION FIELDS

The amount of radiation delivered to a location of interest in a patient by a radiation beam can be estimated from radiation doses measured with the radiation beam incident on a patient-simulating (tissue equivalent) phantom. Measurements can be made using ionization chambers, semiconductor diodes, thermo luminescence dosimeters and radiographic film. Measurements are obtained at incremental depths along the central axis of the radiation beam and expressed as fractions of the amount of radiation measured at a reference location. Depending on the location of the reference dose, these fractions are described as the percentage depth doses (PDD), tissue-air ratios (TAR), tissue-phantom ratios (TPR) or tissue-maximum ratios (TMR). These parameters are provided as data for different radiation beam energies over a range of field sizes and depths in a specified medium. These are used for treatment planning calculations and incorporated in treatment planning systems[17-21].

2.7 ISODOSE CURVES

The absorbed dose in tissue along the central axis can be represented as PDDs, TARs or TMRs. However, dose measurements away from the central axis cannot be obtained from these data. Thus, to estimate the dose away from the central axis, isodose curves are utilized. Each isodose curve defines the absorbed dose as a percentage of the central dose axis at the depth of maximum dose d_{max}[31].

An acceptable treatment plan should (i) give the target volume a uniform dose, (ii) minimise incidental irradiation to normal surrounding tissue, and (iii) ensure dose to any vital organ does not exceed its tolerance level. When a beam passes through a patient, different points will receive different doses. There is a spatial distribution of dose[21]. A point may be designated to receive 100% dose in the irradiated field. Then any other point will receive a percentage *x*% relative to the 100%. Several other points may also receive the same dose of *x*% and this will form an isodose surface. An isodose curve is a result of a line or curve intersecting the plane of the isodose surface. The isodose curves are used to assign dose distribution to the target volume[33]. The isodose curves are a function of the beam quality, SSD, source-to-diaphragm distance (SDD), field size collimation and flattening filters [19].

2.8 COMPUTERIZED TOMOGRAPHY

Computerised tomography (CT) is used as an imaging device for diagnostic purposes in radiation therapy treatment planning. The CT scanner works in conjunction with a laser localization system and a computer graphics workstation. The computer provides capabilities for image manipulation, quantitative information in regard to size and

location of critical organs or inhomogeneities. CT images are used for the localization of internal structures for treatment planning purposes [12, 34-36].

CT scanners generate thin cross-sectional images of the object scanned. In the case of the human body and phantom, the images may be used for diagnostic procedures and radiation treatment planning. CT involves the reconstruction of a tomographic plane from a large number of collected x-ray attenuation measurements during scan mode. X-rays are used for the reconstructing of images in the CT gantry. A narrow bam of x-ray scans across the patient in synchrony with a radiation detector on the opposite side of the patient[35,36]. For a sufficient number of transmission measurements at different orientations, the distribution of attenuation coefficients within the layer can be determined. The CT image constitutes the different attenuation coefficients representing various structures with different attenuation properties. The result of a CT study is a set of transaxial images, which can then be mathematically converted to sagittal, coronal or oblique slices in any plane [12,23].

Reconstruction of the CT image is a mathematical process that generates CT numbers related to the attenuation coefficients. The CT numbers range from -1000 for air to +1000 for bone and water is set at 0.

Normalised CT numbers are called the Hounsfield number H,

$$CT\ number = 1000\left[\frac{\mu_{tissue} - \mu_{water}}{\mu_{water}}\right]$$

Where μ is the linear attenuation coefficient [12, 19]. For dose calculations in radiotherapy planning, the CT numbers are normally converted to electron densities relative to water. The reformatting of CT data produces an image known as a digitally reconstructed radiograph (DRR)[19].

On an image, the CT numbers are given in shades of grey hence providing good contrast imaging. The full set of CT numbers gives a cross sectional image of the object scanned. The slice thickness obtainable on a CT scan is determined by the thickness of the x-ray beam set on the collimator. Typical slice thickness are 1-10mm while scan acquisition times rage from 0.5 to 5 seconds[12]. An initial transmission or pilot scan is useful for survey of patient landmarks and for defining the scan length. This is done by holding the energized x-ray tube in a stationary position while the couch is moving through the x-ray beam as transmission measurements are recorded in the detectors. The measurements are used to generate an image that is similar to the conventional x-ray image. Images are displayed on a computer screen and these can then be digitised into treatment planning computers. CT provides three-dimensional (3-D) images through a series of two-dimensional (2-D) images. Planning target volumes and critical normal tissues can be contoured and manipulated to generate optimised treatment methods on the planning computer[12].

The functions of the CT scanner are[34]:

(i) Localization device, the outlining of the visible tumour volume on all relevant CT slices and possible definition of the Gross tumour volume (GTV) as well

as the clinical target volume (CTV). The location of the target volume can be inferred with reference to a nearby bony land mark or air cavity.

(ii) Diagnosis, which entails scanning so as to obtain qualitative information about irregularities within tissues. A decision on treatment modality, field shape and dose prescription can be done based on information available.

(iii) Normal tissue Localization, observation of normal tissue so as to keep dose as minimal as possible during dose prescription and planning.

(iv) Density data to dose calculations, for purposes of treatment planning by computer, the CT images need to be interpreted in terms of a matrix of attenuation coefficients that can readily be converted to electron densities. This an integral part of the dose calculation by treatment planning systems [34-36,12].

A laser localization system forms part of the CT process and is required to provide reference markers on the patient surface. The isocenter localization is typically calculated within the 3-D volume defined during the pilot study[12]. The target volume that is to receive a prescribed dose is localized and beam geometries are determined and verified prior to treatment on a therapy unit. The simulation emulates the geometry of the therapy unit but uses diagnostic quality x-ray for the localization and verification of treatment position. The images obtained are standard x-ray transmission images with the radiation treatment parameters shown by wire markers as set in the head of the simulator. Real simulation will include emulation of treatment positions, gantry angles, and all other beam parameters required for the treatment[12, 34,35].

2.9 TREATMENT SIMULATION

An important link in the radiation therapy treatment chain is placing of reference marks on the patient so as to facilitate the transfer to further procedures at the treatment unit. A treatment simulator is a machine that uses diagnostic x-ray tube to duplicate a radiation treatment unit in terms of geometry, mechanical and optical properties. The main function of the simulator is to display the treatment fields so that the target volume is accurately delineated and irradiation to surrounding normal tissue is minimised [21,35].

Conventional simulation requires the generation of a diagnostic quality radiograph for comparison with the verification portal image taken during a treatment session. This is useful for the assessment of the positioning of treatment fields. The simulator has an in-built light field that is similar in divergence to the therapy x-ray beam. This light field is used in conjunction with wall-and-ceiling mounted laser to reference markers on the patients surface so as to ensure similar positioning during treatment. In addition, field shaping for blocked fields can be checked on a radiograph taken with the blocks in place. In real simulation, all accessories to be used during treatment should also be employed during simulation[34,35].

For typical 3-D treatment planning, fiducial marks are used as a reference for CT scanning. The exact position of the isocenter is not knows prior to completion of the CT scanning and treatment planning. An approximation of the location of the isocenter is determined form the anterior-lateral pilot view of the patient. Radio-opaque markers (for

example lead strips) are used as external pointers along the CT-slice identified as the patients centre[34].

2.10 TREATMENT VERIFICATION

The problem of ensuring that radiotherapy treatments are carried out as they intended encompasses a multifaceted programme to ensure that treatment delivery is implemented as intended. An assessment of the reproducibility of treatment set-ups and accurate administration of radiotherapy should be facilitated within such a programme. Treatment plans are a result of careful work by the radiotherapist. A dose distribution will have been calculated and at every sep in the process and in the treatment delivery uncertainties will be introduced [37-39]. Uncertainties may include:

(i) Positioning and extent of tumour;

(ii) Inaccuracies in computer dose calculation algorithm;

(iii) Inaccuracies in treatment unit calibration;

(iv) Misalignment of treatment unit;

(v) Patient set-up variations;

(vi) Errors in treatment unit settings.

A comprehensive treatment verification programme should be able to:

(I) Verify dose and treatment plan,

(ii) Verify patient position (i.e. field position),

(iii) Verify treatment machine parameters.

2.10.1 Dose and Treatment Plan Verification

Dose delivery within 3-5% is the acceptable margin. Dosimetric accuracy and precision can be assessed in a number of ways. It is not always possible to achieve considerable certainty that dose measurements are accurate. The pressurised environment of the treatment room where everything must go as smoothly as possible brings in aspects that will require the physicist to be aware of and thereby exercising caution in knowing what accuracy is achievable an avoid the temptation to replace calculations unnecessarily. Precision and accuracy are two aspects that need consideration in dose verification. Precision is the statistical reproducibility of measurements and the resolution of the measuring instrument in use. Reproducibility can be measured by repeatedly measuring under the same conditions and derive the standard deviation *S* from the data[37-43].

The accuracy of a measurement is defined as the deviation of a measurement from the true answer. In radiation dosimetry a number of reasons may contribute to the inaccuracy of a measurement, such as the perturbation of the radiation field caused by the dosimeter and also that the point of measurement may not always be the desired position and inherent dosimeter uncertainties[1-8].

2.10.2 Verification of Positional Accuracy

A number of methods, materials and devices are utilised to ensure patient positioning and immobilisation. These include the use of saggital and lateral lasers, ‘tattoo’ markings on the patient’s skin, an assortment of head and arm rests, as well as chest and footboards. These are used with sole aim of accommodating the variations of patients a radiotherapy

department may have in its care. The simulator provides one of the best means of certifying positional accuracy in relation to anatomy of the patient[6].

The primary aim is to ensure that the position of the radiation beam is as close as possible to the intended location. However, there are a number of limitations to verifications. Firstly, megavoltage beams exhibit inherent poor contrast. It is often difficult to identify a tumour on therapy film. Most decisions are based on bony structure images, which are fairly visible and these are related to the target volume[38].

2.10.3 Verification of Treatment Machine Parameters

Mistakes in treatment parameters occur often enough to cause alarm. Computer based verification of treatment parameters allow for errors to be corrected prior to treatment. Computerized verification systems compare the dose calculated and the set-up parameters with the dose prescription. These are entered into the computer system before hand and are available as reference throughout the duration of the treatment. Although variations may occur from day to day there is an allowance margin within which the parameters can be accepted or rejected by the computer verification system before treatment delivery[30].

In addition, a manual check of the patient set-up is necessary. This includes checking the isocenter position and ensuring that the field size and position are correct. Checking the mechanical operation of the treatment unit is normally done on a daily basis. Beam output parameters are also verified as part of quality control of the treatment unit [30].

2.11 DEVELOPMENT OF PHANTOM

One of the most common cancers in Africa is Cancer of the cervix, therefore pelvic phantom with a "cervix tumour" was designed and built in order to evaluate and verify consistency, accuracy and variability of treatment delivery for cervical cancer. The phantom was designed and fabricated for imaging, localisation, and treatment planning (dose calculations) and dose delivery applications in performing quality assurance for treatment delivery. The implementation of radiotherapy involves the expertise and application of several skills such as imaging, localisation, dose calculations, treatment planning skills and software, radiation dose measurements and delivery systems. Therefore, with all these parameters in place it is necessary to have a realistic assessment of the uncertainties incurred as a result of the various stages involved. Each of the skills mentioned above contribute to the final number of uncertainties and thus a phantom to assess these skills is desirable[6].

Treatment of cancers at various anatomical locations has spurned a variety of phantoms and protocols used for assessment. It is desirable to know exactly what the dose is delivered to the tumour volume while maintaining the dose to normal tissue or organs at risk at minimal or accepted levels. The higher treatment accuracy required for dose calculations introduces more stringent requirements on the methods used for treatment delivery and checking of treatment plans[42-47].

The material selection criteria is based on radiological properties of the materials. Radiological test was done based on images obtained on film and CT scanner.

2.12 RATIONALE FOR DEVELOPMENT OF PHANTOM

Phantom design and fabrication based on the following:

(i) Imaging

(ii) Demarcation of treatment volume and margins

(iii) Treatment planning applications

(iv) Treatment delivery verification

(i) Imaging System Verification and Inter-comparison:

- Phantom designed to provide a standardized configuration of organs with well-defined dimensions of the cervix and rectum fabricated with realistic tissue equivalence.
- Images of phantom from computed tomography, simulator or port films compared to verify consistent geometric registration by each of the different imaging modalities.
- Rigid construction of phantom and plat surface provides easily achievable reproducibility of the phantom positioning. This is necessary for evaluation of the imaging system[1-6, 37-47].

(ii) Delineating Treatment Volume and Margins:

- Anatomical representation and dose calculations
- Routine treatment planning use of different anatomical representation is familiar. A 2-dimensional planning system is used to define the tumour volume.

- CT-based density values are useful for dose calculations especially in the case of inhomogeneities[1-6, 12].

(iii) Treatment Planning Applications

- Positioning of phantom on the simulator in the treatment position with the appropriate immobilization devices (if required) and verification of setup of the isocenter using beam's eye view (BEV) or digitally reconstructed radiograph.
- Representation of phantom anatomy should be visible on simulator film.
- Check of the location and orientation of each planned treatment fields using BEV and /or DRR methods[1-6].

(iv) Treatment Delivery Verification

- Treatment on the linear accelerator (linac).
- Use of 'cut' port films and thermo Luminescence dosimeters (TLDs).
- Phantom is fabricated to place the film and TLDs in the region of interest. Imaging of the phantom during irradiation allows precise localization of the detectors and thus a better comparison of the measured and calculated data.
- Comparison of human CT-number and the phantom CT-number for tissue, bone and rectum[1-6].

3. METHODOLOGY

3.1 CHARACTERIZATION OF PHANTOM MATERIAL

3.1.1 Physical Properties

The materials used to fabricate the phantom are used locally within the hospital. This brings in the aspect of cost effectiveness and therefore making it possible to keep costs as low as possible. An important aspect of the materials used was to consider their physical properties so as to differentiate them in relation to their representation of the human body. The four materials selected for investigation was done based on available data and previous studies. The four materials investigated were acrylic, aluminium, plaster of paris and dental wax.

The intention was to investigate the possibility of using the above mentioned materials as human tissue substitutes and based on this a number of properties were investigated. The Physical properties investigated include: the physical density, the electron density and the effective electron density. The formulae used are given in appendices A and B. Attenuation characteristics were investigated as a radiation absorption property[48-50].

3.1.2 Acrylic

Acrylic is one of the materials recommended, by various authors, as suitable for making phantoms used in radiotherapy dosimetry. Chemical formula is given as $C_5H_8O_2$. . Cross sectional area of the acrylic sheets used was 32cm x 25.5cm and a thickness of 6mm. Acrylic was investigated for suitability as a soft tissue substitute.

3.1.3 Aluminium

Aluminium (Al) sheets of 8mm thickness were used for characterization purposes. Al was chosen as a bone substitute and was investigated for similar properties to bone thereof. Physical density, electron density and attenuation coefficient of aluminium was compared to that of bone to check for compatibility.

3.1.4 Plaster of Paris (Gypsum)

Gypsum is hydrated calcium sulphate ($CaSO_4{:}2H_2O$). A paste made by mixing one part water to three parts of powder calcium carbonate and molded into blocks of various thickness for attenuation characterization of the plaster of paris (P.O.P). The thickness ranged from 1.25 cm to 6.3 cm. Cross sectional area of each block is 22.6cm x 22.2cm.

All the blocks were left to dry for approximately two (2) days before any measurements were made. To test for dryness, the colour of the blocks served as an indicator of how dry the blocks were and also a dampness test with paper placed onto of the blocks. The paper served to absorb moisture lost from the P.O.P. blocks. The variation in thickness of the blocks served to provide attenuators of differentiable thickness to maximum of 10.2 cm.

3.1.5 Dental Wax

Dental wax is a combination of various paraffin waxes and beeswax. Its general chemical formulae is C_nH_{2n+2}; where n can take on values 20 – 35. Wax is fairly easy to mould or cast into any shape thus making it easy to handle. It is a good soft tissue or

muscle substitute[26]. Its suitability as a phantom material is within reasonable doubt and therefore its choice of use has been based on its radiological properties in comparison with the other materials used. Based on testing for radiological contrast, one can ascertain the suitability of a material for investigation purposes. Physical dimensions of dental wax sheets used for attenuation calculations are 18.92cm x 8.8cm x 0.78cm.

3.1.6 Material Selection Criteria

In order to assess the performance of the different substitution materials, it was necessary to compare them with the biological material they are intended to represent. The parameters used for comparison are:

(i) The mass attenuation coefficient,

(ii) The electron density and

(iii) The effective atomic number.

3.1.7 Attenuation Characterization

Attenuators are normally used as beam modifiers in radiation therapy. Based on the same principle, attenuation characteristics for the materials are determined for purposes of comparing attenuation capabilities and qualifying the material in terms of their attenuation properties. The attenuation curve depends on the geometric relationship between the radiation beam, the attenuation medium and the detector [19]. Narrow beam (good) geometry was used to determine the attenuation behaviour of the materials.

In this se-up, the scattered photons emanating from the attenuating medium will not contribute to the detector reading. Therefore the detector reading will almost be entirely due to the primary photons that travel through the medium without any interaction.

The attenuation coefficient obtained from narrow beam geometry is a unique value for each material. Narrow beam transmission measurements were carried out using two photon beam energies, 6MV and 10MV. The equipment used was:

- Siemens KD linear accelerator (Department of Radiation Oncology, Pretoria Academic Hospital),
- Ionization chamber, for dose measurement.
- PTW Unidos electrometer.

The chamber is placed in a column-shape hole in the phantom of square cross section of 20cm x 20cm x 30cm, which was large enough to ensure lateral electronic equilibrium. The attenuators were placed on a 1.2cm acrylic tray on the treatment couch. Narrow beam geometry is achieved by a large source-detector-distance (SDD). All measurements are made along the central axis of the photon beam. It has been reported by other authors that narrow beam geometry yields similar results as extrapolated broad beam measurements[50]. Therefore in this investigation only narrow beam geometry is considered. Experimental setup of the narrow beam geometry is shown in figure 6 below.

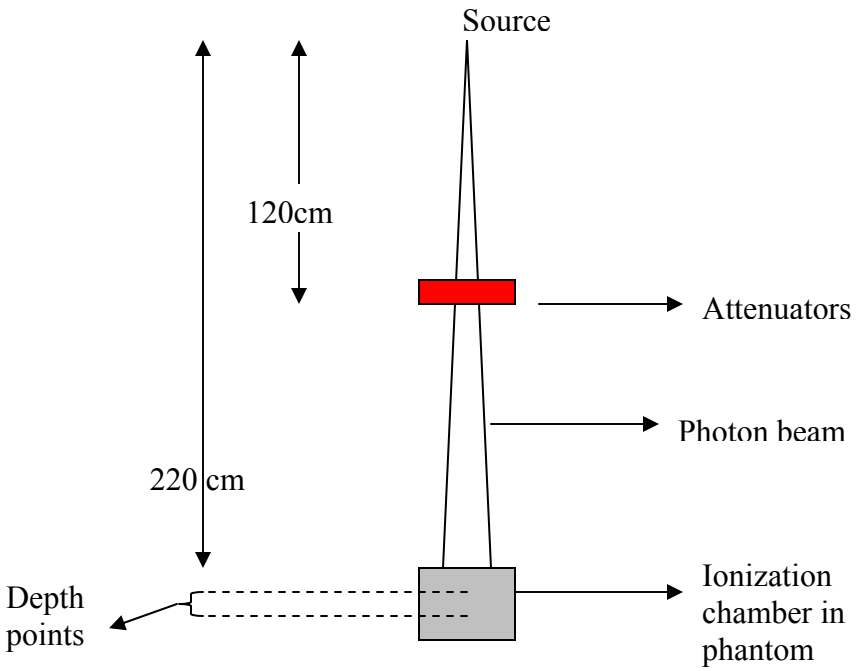

Figure 6 Schematic set-up for attenuation measurements

Ionization chamber measurements made at a distance of 220cm from the source. The chamber was situated at two different depths of 1.2cm and 5cm. . Ionization chamber readings are normalized to the measured value obtained with only the Plexiglas tray in the path of the beam (i.e. assumed as no attenuator in path of beam). Collimator opening set at 2cm x 2cm and thus defining the field size at machine isocenter. A transmission factor (T) defined as the ratio of the chamber reading at a depth in the phantom without the attenuator (I_0) to the reading with the attenuator (I) is used to determine the narrow beam transmission and in effect derive the effective linear attenuation coefficient μ_{eff} according to the following expression

$$T = I / I_0 = \exp(-\mu x) \qquad 3.1$$

X is the thickness of the attenuators.

The effective attenuation coefficient is calculated form the expression

$$\mu_{eff} = \Sigma\, \mu_i \qquad 3.2$$

Where μ_i is the attenuation of a slab of thickness x_i.

The effective attenuation coefficient is intended to reflect variations of the non-monoenergetic beam, the thickness *x*, field size and the depth in phantom.

3.2 PHANTOM FABRICATION

Individual 12mm thick Perspex slices where machined with a configuration based on

(i) Pelvis section of anthropomorphic phantom at Pretoria Academic Hospital, department of radiation oncology.

(ii) CT slices from patient files to obtain an ideal location and typical volume of cervical cancer tumour.

External contour and internal contours of organs of fabricated phantom based on anthropomorphic phantom dimensions. Materials used are Perspex for soft tissue, wax for the tumour volume and rectum, plaster of paris for the left and right femurs of the pelvis.

The bones (left and right femur) are fixed in place and are not movable. The central part of the phantom is made to accommodate a tumour volume inside a circular insert. Three inserts have been fabricated. Insert one (1) is the tumour insert or diagnostic module (figure 7 below); two (2) and three (3) are the dosimetric inserts or therapeutic module. Insert 1 is the imaging modality and inserts 2 and 3 are for treatment delivery verification. Inserts 2 and 3 are both designed to accommodate therapy verification film

and TLDs. The variation between two and three is the placement of the dosimeter detectors. Insert 2 has the film and TLDs placed at the top of the pyramid whereas insert 3 has the TLDs and film placed at the lower end.

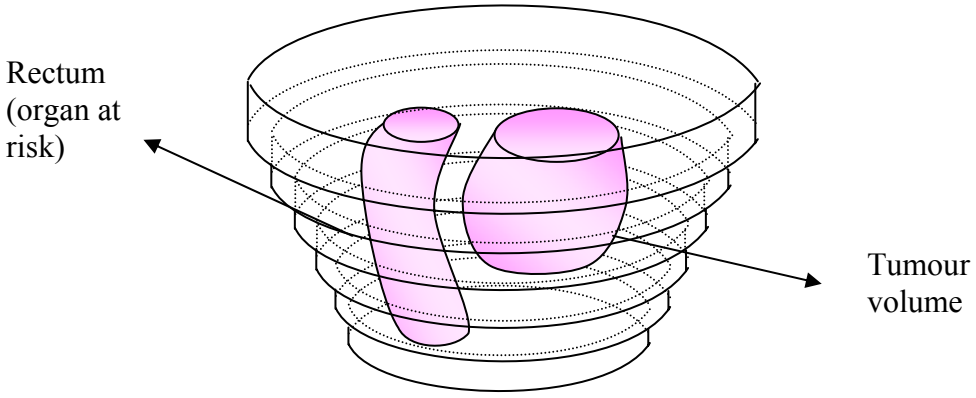

Figure 7 imaging diagnostic modality insert 1.

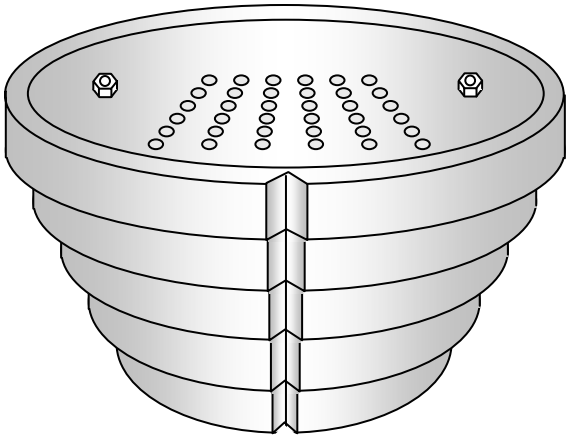

Figure 8 Dosimetric insert 2 and 3

Figures 9 and 10 below show the variations in placement of the dosimetry tools i.e. film (fig. 9) and the TLDs (fig. 10)

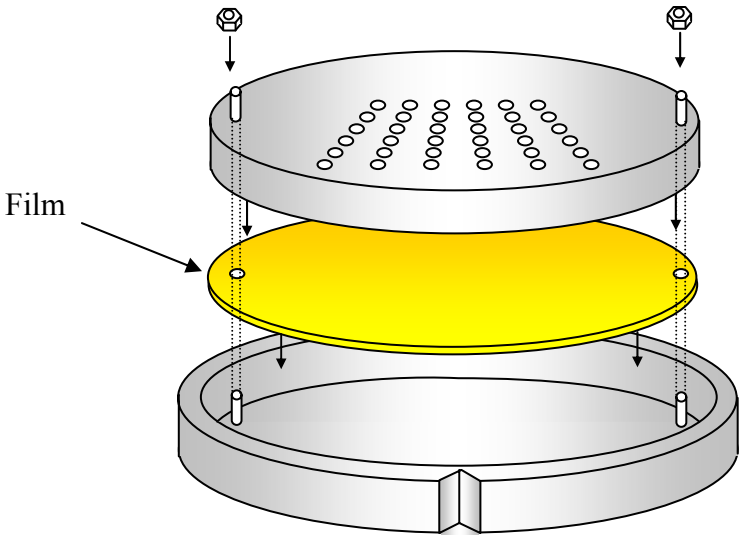

Figure 9 Film cartridges.

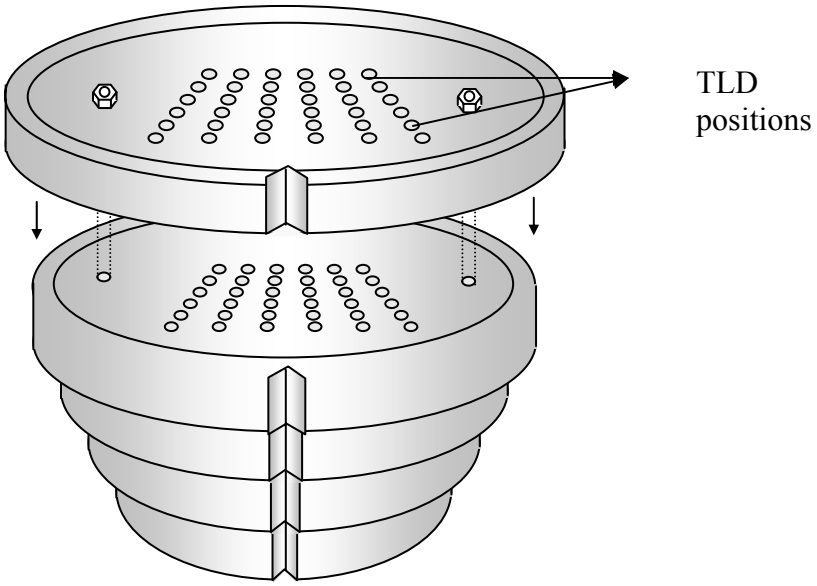

Figure 10 TLD holders

3.3 LIGHT PROOF TESTING OF THERAPY INSERTS 2 AND 3.

Due to the sensitivity of film to natural light, it is necessary to ensure that film that is to be used is kept out of natural light and that the film is kept light tight. This entails light proofing film prior to and after exposure to radiation. A number of precautions come into play for film used for dosimetry of therapeutic radiation. Radiotherapy dosimetry films are usually individually pre-packaged in lightproof paper for convenient use without the need to load in a cassette loading system. These can be used in direct light without darkening or in red light. In the case of use in anthropomorphic phantoms and also for use in the cervix phantom designed, it is necessary to cut and shape the film to the desired shape for ease of use. This is done with the caution of sealing the edges with black tape so as to block out natural light.

Taking into account that cutting the film creates artefacts; an investigation of this effect becomes necessary. To test the effect of cutting the film, low energy film cut into similar shaped disks as the ones to be used in the phantom inserts. Holes punched into the film for purposes of creating a comparison basis for cut and uncut film.

Lightproof testing of phantom inserts is done by cutting disks of film and placing them inside the circular film cartridge. The design of the film cartridge necessitates punching holes into the film for a perfect fit. The holes are punched inline with the guide screws for the film cartridges. The inserts are left for 24 hours in a room illuminated by a florescent lamp thereby exposing the film to light.

3.4 Film Dosimetry

Film dosimetry served as a quality detector for radiation. This emanates form the fact that film gives a picture of the spatial distribution of a radiation beam at a specified point. Attenuation information is obtainable as an image. Film was also used as a quantitative dosimeter because it allows for determination of two dimensional dose distribution and a measure of the total dose.

Film dosimetry requires the use of a density versus dose curve (DDC). Optimum measurements conditions are in the linear part of the curve. Dose response of the films was investigated under various irradiation conditions. Irradiation conditions include the film parallel to the beam and perpendicular to the beam. A polynomial fit of the optical density is plotted to convert density to dose.

3.4.1 Film calibration

X-omat film pre-packaged in lightproof paper is used for calibration. The setup used is shown in figure 11 below.

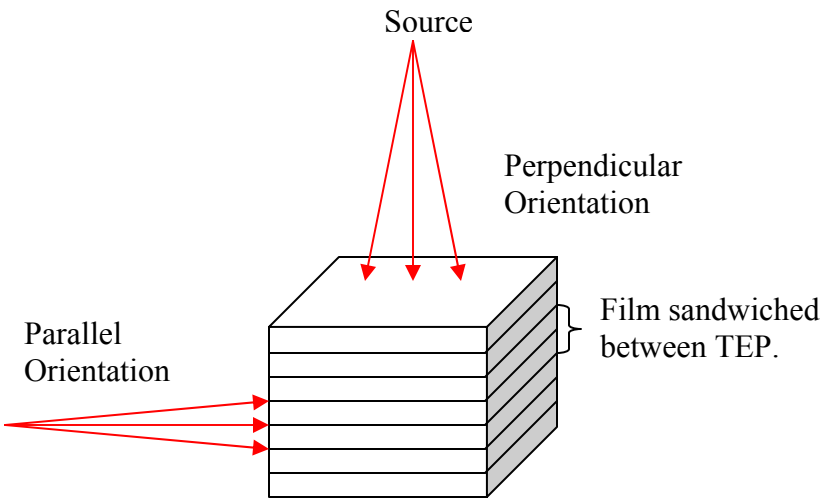

Figure 11 Film calibration set up.

The two irradiation configurations are shown in the figure above. For the perpendicular configuration, film is placed at a depth of 5cm at isocenter. The parallel configuration has the film sandwiched between the TEP and is parallel to the radiation beam. Field size defined at the isocenter is a 10 x 10 cm^2 and 70 –90 monitor units were delivered at SSD=100cm and a calibration curve obtained for different monitor units.

3.5 THERMOLUMINESCENCE DOSIMETRY (TLD)

Lithium Fluoride (LiF) thermoluminescent (TL) chips were used for point dose measurements. All chips were calibrated in order to determine the Element Calibration Coefficients (ECC) for each dosimeter. Dosimeters were either rejected or accepted by the processing software depending on whether the ECCs where within acceptable limits. All dosimeters correction factors were generated by the software and incorporated into the subsequent readings to correct for the fading characteristics and wear of the TLDs. Reader correction values and standard deviations were also calculated for each TLD by the software and therefore all subsequent readings were in effect already corrected for by the software. A batch of 66 TLDs was used.

Calibration Procedure:

(i) C*alibration:* to determine the TL response of a dosimeter used to measure exposure or absorbed dose of a clearly defined energy. Calibration done for 6MV and 10MV photons. TLDs calibrated against a calibrated ionisation chamber for a known energy. Calibration done at isocenter for a 10 x 10 cm field size. Nominal output of linear accelerator recorded for reference

purposes and also to establish any fluctuations in machine output. Build-up material is used around the TLDs in order to achieve electronic equilibrium. Calibration conditions made identical to measurement conditions as closely as possible in terms of depth, photon beam energy and same treatment machine.

(ii) *Measurement of Irradiation:* measurement of actual exposure or absorbed dose in phantom and used to determine dose delivered.

Instrumentation:

Essential features of the TLD reader are:

(i) a heating system;

(ii) a light detection and collection system;

(iii) a signal and measuring system, and

(iv) A display and recording system.

Figure 12 depicts the main features of a TLD reading system.

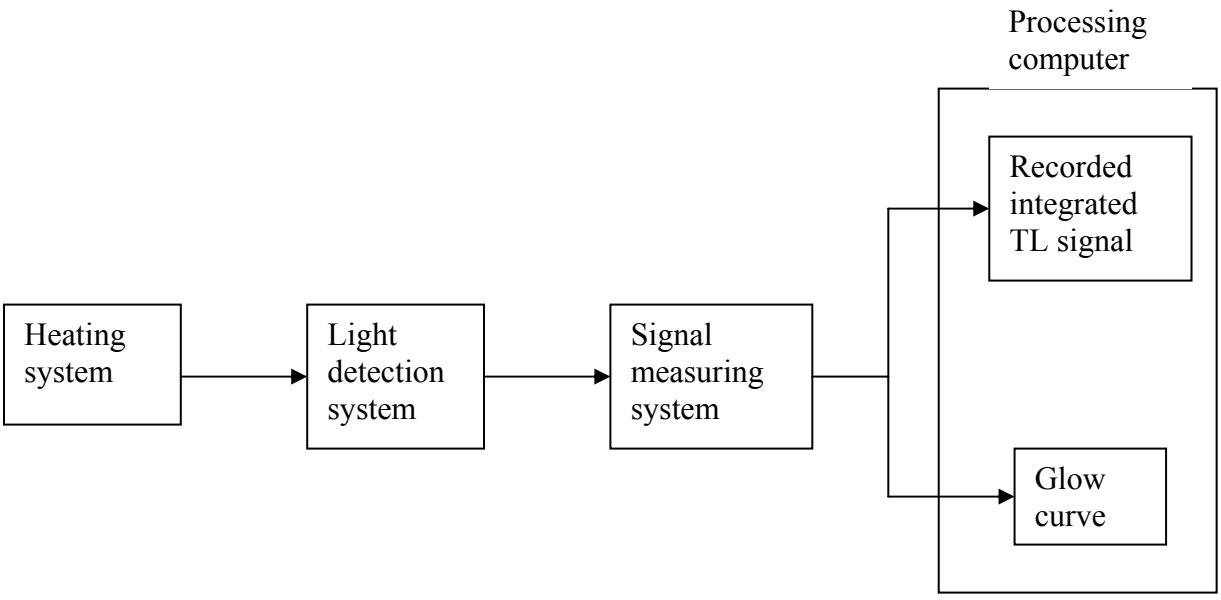

Figure 12 Representation of the main components of a TLD reader.

TLD was signal read using a Harshaw TLD reader. The TLD chips were read out one at a time placed on a heater planchet and heated to a maximum of 300^0C in approximately 50 seconds. The TLD reader periodically performed light and noise background checks. TLDs had to go through a pre-irradiation anneal at high ($\pm 300^0$C) and low ($\pm 100^0$) temperature over night in a programmable anneal oven. Post irradiation anneal of TLDs automatically performed in the TLD reader during readout of TL signal. A glow curve is measured for each TLD that is read and this is displayed on screen with its corresponding TL response in nanocoulombs (nC). Dose delivered is calculated based on the machine output calibration which can be compared to ionization chamber measurements. TLDs are sorted and a calibration file is created for each batch depending on the number of monitor units set to deliver a dose. Each TLD is labeled and assigned a unique calibration factor. The TLDs are exposed to a know dose and an Element Correction Coefficient (ECC) is generated by the reader for each TLD chip to account of sensitivity variations. A reader calibration factor (RCF) within the TLD reader software is used to convert measured signal into dosimetric units. Direct dose measurements for treatment verification are given by the equation:

Dose (Gy) = Reader output (reader units) X RCF (Gy/reader unit) x ECC

The TLD dose readings are tested for the following parameters:

(i) Background and light test signals at intervals of 20 readings.

(ii) The standard deviation of the TL signal for calibration.

(iii) The agreement between measured and predicted dose values.

3.6 TREATMENT VALIDATION

Below is a schematic representation of the procedure followed in order to demonstrate the verification principle used.

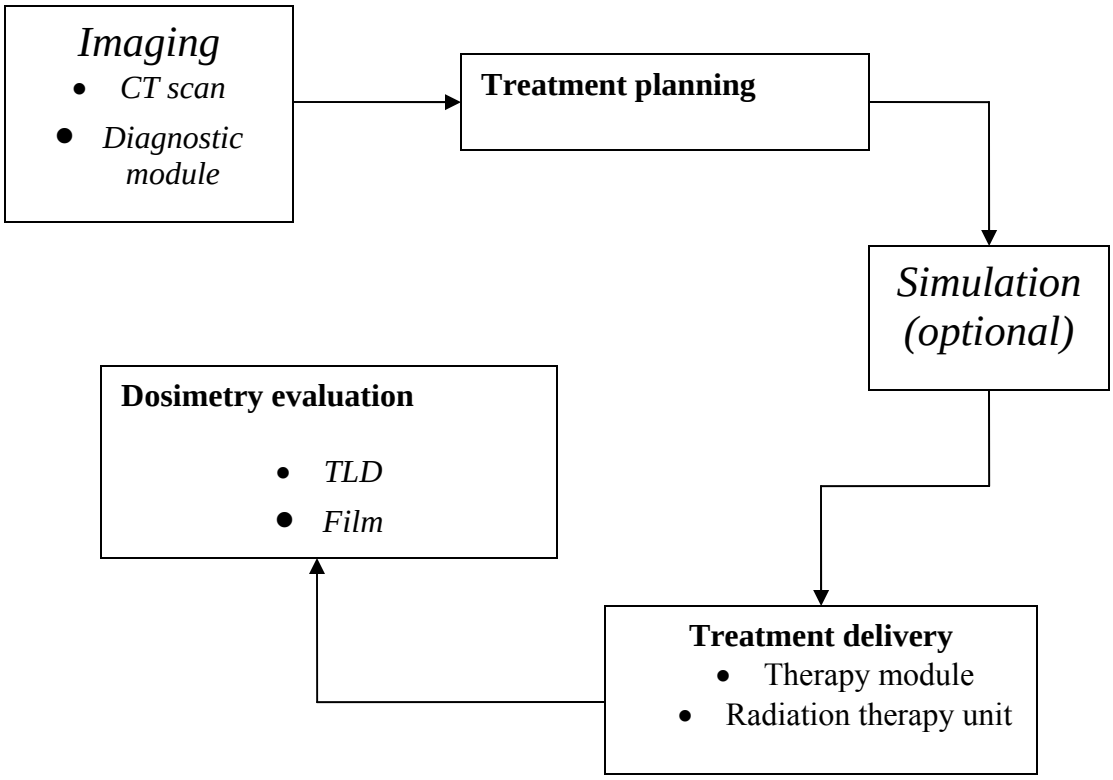

3.6.1 Imaging and Treatment Planning

Image-based treatment planning requires that the data be acquired in the treatment position. Volumetric data are acquired with slice thickness of 1 cm on the CT scan. Volumes of interest to be delineated are the Gross tumor volume (demonstrated tumor) and the Clinical Target volume (larger than the tumor volume). The planning target volume encompasses the clinical target volume and an additional margin to cater for inaccuracies in the beam and patient set-up[52].

Three typical cervical cancer treatment techniques where planned for the phantom; namely anterior-posterior/posterior-anterior, rotational therapy and four-field therapy. The treatment planning system uses the convolution algorithm to calculate the dose distribution prescribed. CT images are manually contoured into the planning system. Dose distribution and treatment configurations determined are by the treatment planning system. Dose calculations are based on CT data acquired with a CT scanner (Picker IQ Fast). Interest point doses are required for TLD absolute dose determination. Interest point doses randomly selected based on actual matrix array in the phantom and are selected depending on the area of interest. Dose distribution is determined using film dosimetry with the film disks placed at different levels in the phantom.

Normalization dose is to a 100% and dose is prescribed to a global maximum of ±70 cGy. This is so due to the fact that for film analysis purposes, a dose beyond 70 cGy will saturate the film which is not particularly ideal for determination of optical densities. All other beam parameters are obtained from the treatment planning sheet and are reproduced under treatment conditions. Three treatment methods were used; they are arc or rotational therapy, four-field and anterior-posterior/posterior-anterior (AP/PA).

3.6.2 Simulation and Treatment

The phantom was placed on the couch of a simulator and position according to the laser alignment system in the room as well as the reference marking on the phantom done at the CT scanner. The following steps were followed:

- Phantom positioned according to treatment sheet.

- Location of simulator isocenter according to phantom thickness. Phantom position is viewed on a fluoroscopy screen and any couch movements can be verified on-screen.
- Treatment beam location was done with phantom in treatment position. Couch parameters recorded.
- Treatment beams are simulated with simulation film for each treatment field.

The phantom was placed on the treatment couch for each treatment and positioned according the marks made at treatment simulation. Each treatment method required the use of 65 TLDs and 5-9 film disks. TLDs and films were placed inside the phantom during treatment and were then analyzed after each treatment with their specific analysis instruments. Each treatment was done at least twice because of uncertainties in positioning. An average of the readings is reported for the respective dosimeters**.** Table 1 below gives a summary of the set-up parameters as predicted by the treatment planning system.

Table 1 Treatment set-up parameters.

Treatment description: Parallel opposed Anterior Posterior		
Orientation	Anterior	Posterior
Set-up: SAD **SSD**	100 cm 89.6 cm	100 cm 89.6 cm
Field definition: **Width**	 10 cm	 10 cm

Length	15 cm	15 cm
Depth	10.4 cm	10.4 cm
Monitor units	36	35
Treatment description: Arc Therapy		
Orientation	Beam 1	Beam 2
Set-up: SAD **SSD**	100 cm 89.6 cm	100 cm 89.6 cm
Field definition: **Width** **Length**	 9 cm 15 cm	 9 cm 15 cm
Arc rotation	135	135
Treatment aids	45^0 wedge	45^0 wedge
Weighting (cGy/no. of fractions)	33.0 / 1	33.0 / 1
Depth	13.3 cm	13.3 cm
Monitor units	105	105

Treatment description: Four field				
Orientation	Anterior	Posterior	Right Lateral	Left Lateral
Set-up: SAD **SSD**	100 cm 92.6 cm	100 cm 86.5 cm	100 cm 82.3 cm	100 cm 82.4 cm
Field definition:				

Width **Length**	11 cm 15 cm	11 cm 15 cm	9.5 cm 15 cm	9.5 cm 15 cm
Treatment aids	Customised block	Customised block	Customised block	Customised block
Weighting (cGy/no. of fractions)	20 / 1	16 / 1	15 / 1	15 / 1
Depth	7.4 cm	13.4 cm	17.7 cm	17.7 cm
Monitor units	22	20	22	22

3.6.3 Thermoluminescence Dosimetry Technique

66 TLDs were processed per treatment technique and were placed at the interest dose points within the phantom. After each treatment irradiation, the TLDs had to undergo through a pre-read and post-read annealing. The TLDs were read in a TLD reader (Harshaw) which stores the calibration properties of individual TLDs and thus providing individual calibration factors for each TLD as per energy type. The TLD reader was connected to a processing computer (PC), which analyses each TLD reading and displays the glow curves and provides a dose reading. Each TLD was individually identified as per number and position within the phantom and dose measured was reported in centigray (cGy).

3.6.4 Film Dosimetry Technique

This requires film to be cut into circular disks that can fit into the film cartridges within the phantom making sure air pockets are removed. The phantom is placed on the treatment couch and positioned with respect to the x-ray therapy beam using the light field to ensure coincidence with the markings on the phantom and the lasers to guide the set-up. The phantom is exposed according to the treatment protocol and is exposed to a maximum dose not more then 70cGy (66-70 cGy) so as to simplify analysis and avoid the non-linear response region of the optical density-to-dose response of the film.

A calibration film was developed for determination of the HD curve. An Unexposed film was developed in the same processor as the exposed film and at essentially the same time to provide a null dose reading. Film analysis for isodose distribution is performed on a film dosimetry system (RIT113). The software generates the HD curve to use for each film batch that is processed. Film dosimetry is used to determine dose distribution (in percentages) for each of the treatment methods.

3.6.5 Treatment Verification

Treatment planning system calculated dose and TLD measured dose were computed and compared according to the equation

$$\text{Percentage Dose Difference} = \frac{Dose_{TPS} - Dose_{TLD}}{dose_{TPS}} \times 100\%$$

Criteria of acceptability are anything between ±5%. This will be considered as a clinically acceptable tolerance level according to what is available in literature. All

treatment plans are verified by in-house dose check program. The TLD readings are divided into high dose gradient and low dose gradient readings.

Dose distribution analysis is a quality index of the treatment method and is qualifies as very good, good and poor depending on the dose distribution patterns observed on film and position of the isodose lines of interest.

4. RESULTS

4.1 Characterization of Material

4.1.1 Physical Properties

The physical properties calculated are physical density, the effective atomic numbers and the electron density. Actual values used in the calculations are given in appendix D. The physical properties are listed in table 1.

Table 1 Physical Properties.

Material	**Chemical formula**	**Effective atomic number**	**Physical density ($g.cm^{-3}$)**	**Electron density (N_e/g)**
Plaster of Paris	$CaSO_3$: $2H_2O$	11.3	1.43	4.47×10^{23}
Perspex	$C_5H_8O_2$	6.56	1.25	3.59×10^{23}
Wax	C_nH_{2n+2}	5.42	0.86	4.68×10^{23}
Aluminium	AL	13	2.69	2.902×10^{23}

4.1.2 Material Selection

The materials selected for construction are acrylic, dental wax and plaster of paris. The choice of material is based upon constraints of cost effectiveness, availability and easy of construction. Aluminium proved to be more costly in comparison with the other materials and also more difficult to handle in terms of cutting and shaping into required shapes.

4.1.3 Attenuation Characterization

Attenuation characterization was done with respect to three (3) photon beam energies for a long source-to-detector distance and field sizes ranging from 1x1 to a maximum of 6x6. Table 2 gives the averaged results obtained for calculated attenuation coefficients.

Table 2. Variation of atomic number and attenuation coefficient

Material	**Effective atomic number Z_{eff}**	**Effective attenuation coefficient μ_{eff}**	**Mass attenuation coefficient (μ_{eff}/ρ)**
Plaster of Paris			
6MV	11.3	0.066	0.046
10MV		0.065	0.045
Acrylic			
6MV	6.56	0.052	0.042
10MV		0.039	0.031
Wax			
6MV	5.42	0.042	0.048
10MV		0.035	0.041
Aluminium			
8MV	13	0.90	0.33

The results presented above are based on measurements taken with an ionization chamber and are therefore subject to inherent uncertainties of the measuring device. The results give a clear picture of the difference in attenuation characteristics of the materials and thus are favorable for use in depicting the anatomies that were intended for the phantom.

Below (figure 1) is a representative sample of the attenuation curves obtained for the four materials investigated. The largest and smallest field sizes are plotted in order to facilitate discussion. Further data is obtainable in appendix D5, which gives all data for the various field sizes and photon energies.

Attenuation curves as a function of field size and photon energy

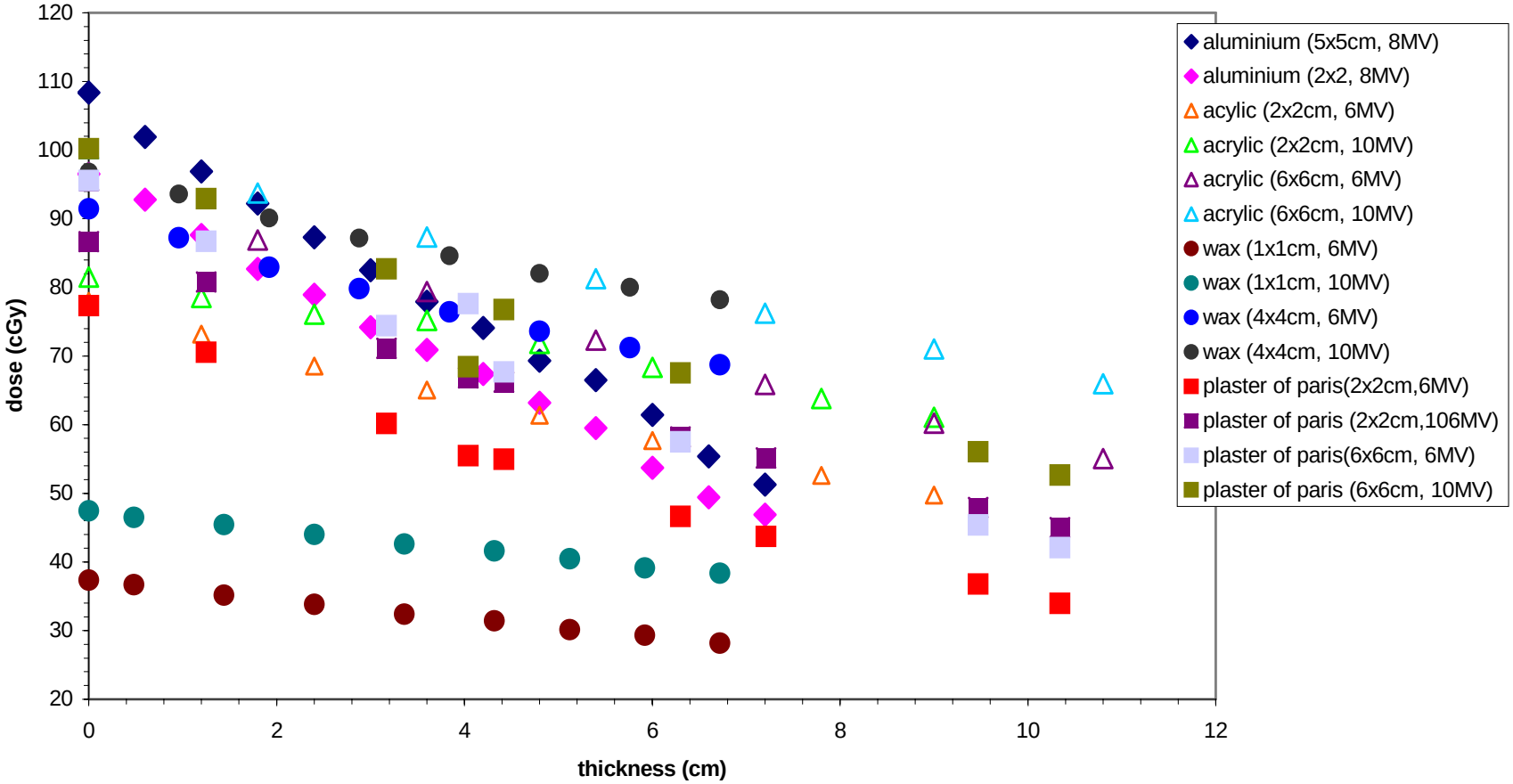

Figure 1 Attenuation curves for acrylic, aluminium, plaster of paris and wax.

4.2 Phantom Fabrication

The phantom has successfully been constructed to with the following capabilities:

- Imaging through CT and simulator,
- Demarcation of treatment volume,
- Treatment planning applications, and
- Treatment delivery.

The phantom was constructed of acrylic soft tissue, which formed the outer contour of the pelvis, plaster of paris bones and dental wax tumor volume and rectum. A photograph of the phantom is given below in figures 2A and 2B.

Figure2A Picture of phantom with diagnostic module inserted.

Figure 2B Photograph of phantom with field size markings.

Figure 3A and 3B below are the diagnostic and therapy inserts respectively.

Figure 3A photograph of diagnostic insert.

Figure 3B Therapy insert

4.3 Lightproof Testing

Lightproof testing proved successful and useful as it provides evidence that the film cartridge coating was enough to block out normal light. The light proof testing was done for the therapy module (figure 4). This is an important aspect if film is to be used for dosimetry. Radiographic light is made such that it should not be exposed to any light other than dark room lighting before exposure to radiation. All film loading and unloading is done in the dark room.

4.4 Film dosimetry

Film response is determined as a function depth for a fixed field size (10cm x 10cm), SSD of 100cm for a 10MV photon beam. Film response is reported in terms of optical density versus dose from which a dose calibration or H-D curve is determined (figure 4). A single calibration curve (selected form a sample of 3 different films of 70, 80 and 90 monitor units.) was used to process all other films used. Any uncertainty in the optical density is converted to the uncertainty in the absorbed dose measured through the calibration curve. The processing software and computer is able to use one calibration film for more than one film. The curve is linear for the dose range of 0 –70 cGy.

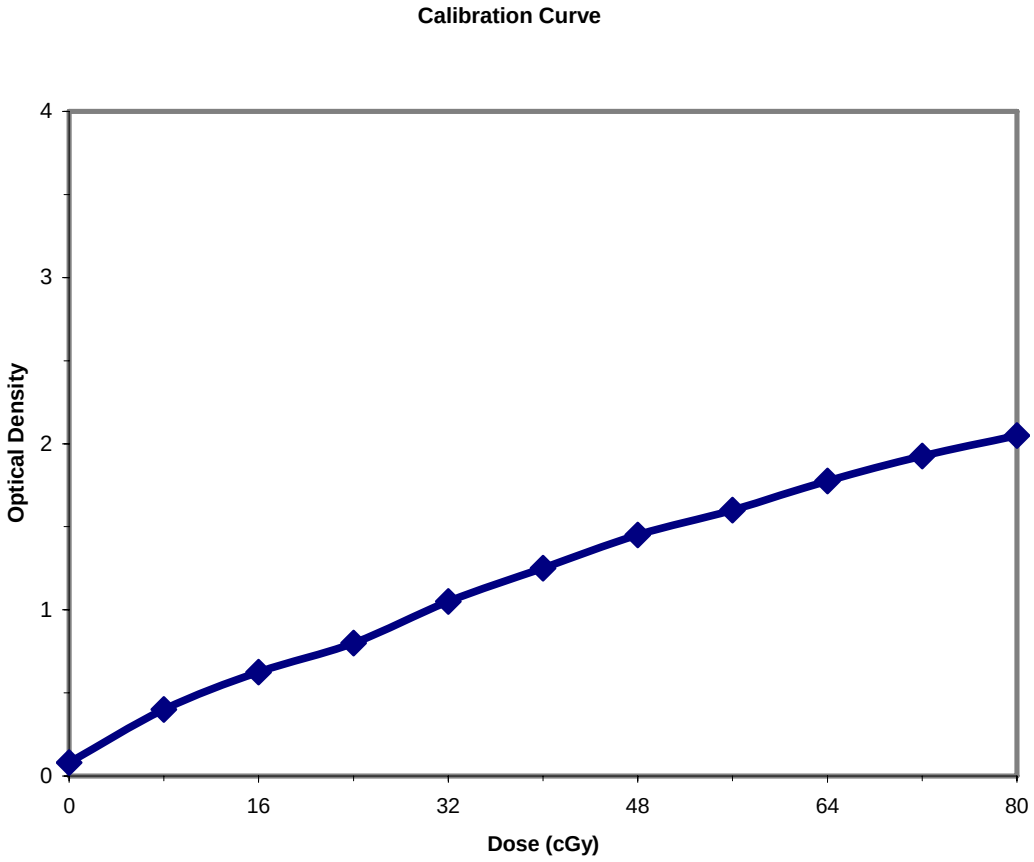

Figure 4 Calibration curve for 70 Monitor units

4.5 TL Dosimetry

The TLDs used in this study were calibrated for a response per unit dose normalized to 10, 30,50, 70 and 100 cGy. Five groups of TLDs were irradiated to the aforementioned doses by nominal 10MV photon beam. All TLDs were placed at depth of dose maximum (d_{max}) and exposed to the chosen number of monitor units. Nominal output of treatment unit was within expected range prior to irradiation of TLDs. Calibration curve is shown in figure 5 below.

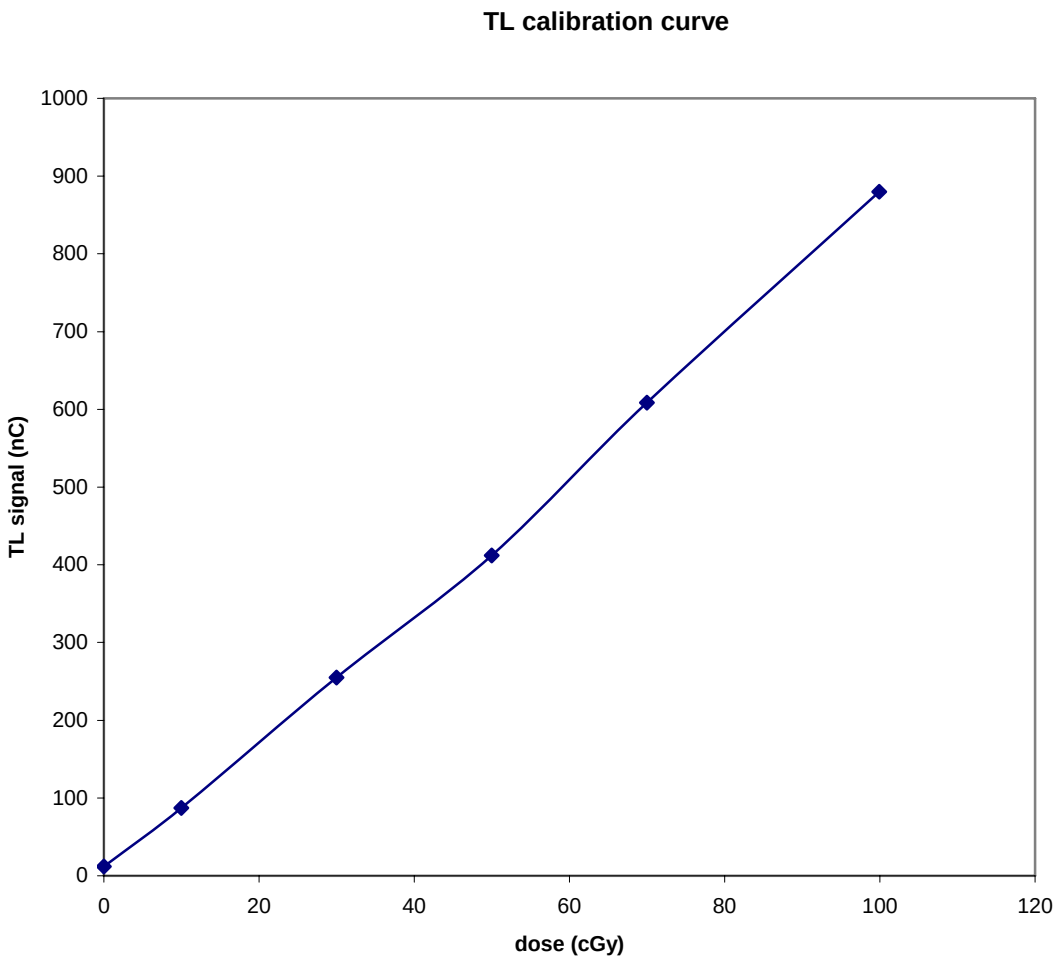

Figure 5 TL calibration curve

TLD response is linear in the energy range 10-70 cGy. The mean standard deviation over the range is 4.3 with a range of 3.26 – 6.06. Each TLD reading was corrected for sensitivity of the TLD reader (RCF) and applied elemental correction coefficient (ECC). The larger ECC correspond to lower dose readings. Background noise and light test was periodically performed after 20 TL readings. The signal for an unexposed TLD was typically in the range of

4.6 Treatment validation

4.6.1 Imaging and Treatment planning

CT scan images were obtained and the CT data transferred to the treatment planning system. CT images were obtained under normal pelvis examination protocol. Good contrast is observed and a clear indication of the demonstrated tumour volume as well as clear TLD positions (figures 6 and 7). The CT scans show good contrast between the bone structure (plaster of paris), soft tissue (acrylic) as well as the demonstrated tumour and rectum (dental wax).

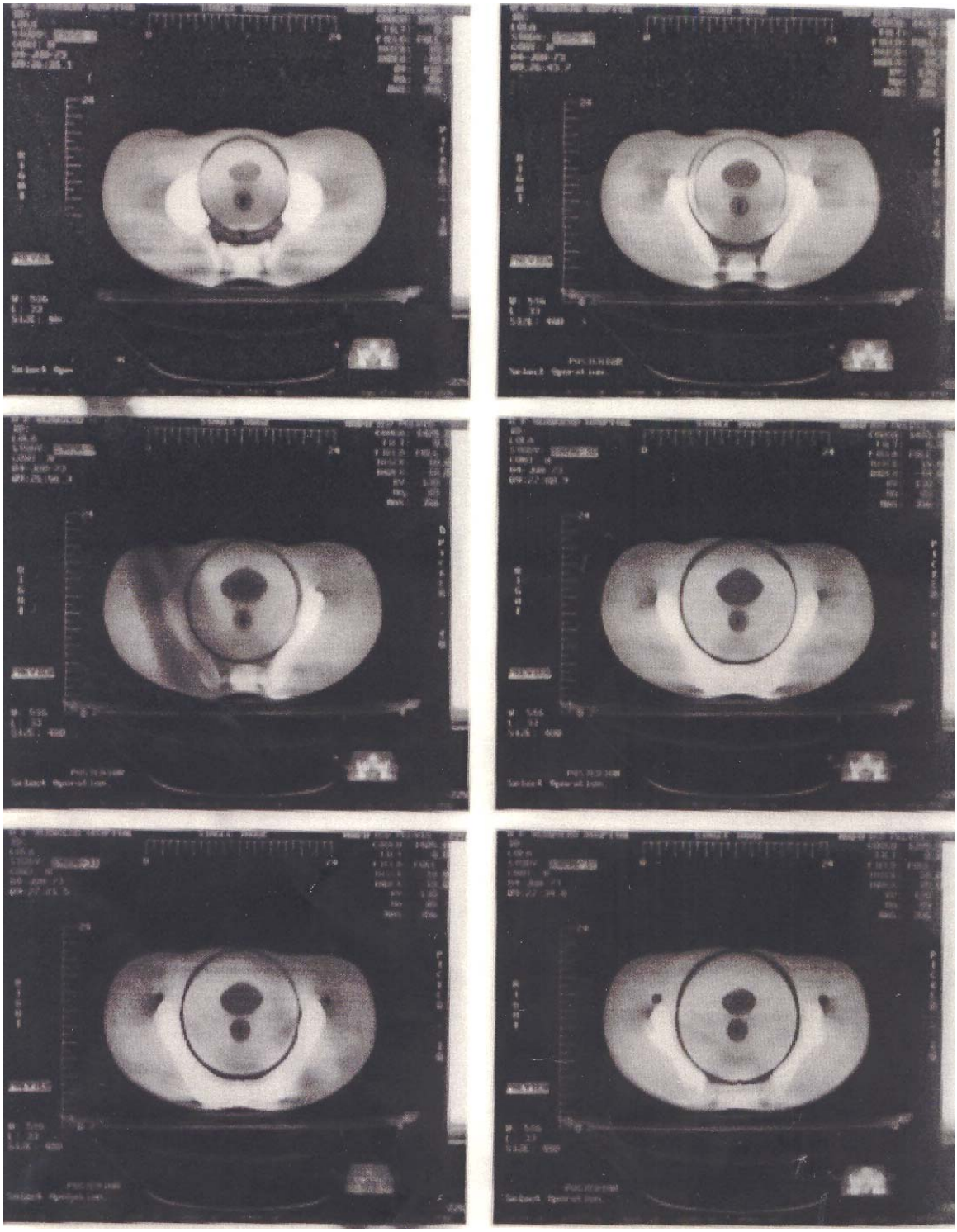

Figure 6 CT diagnostic module image.

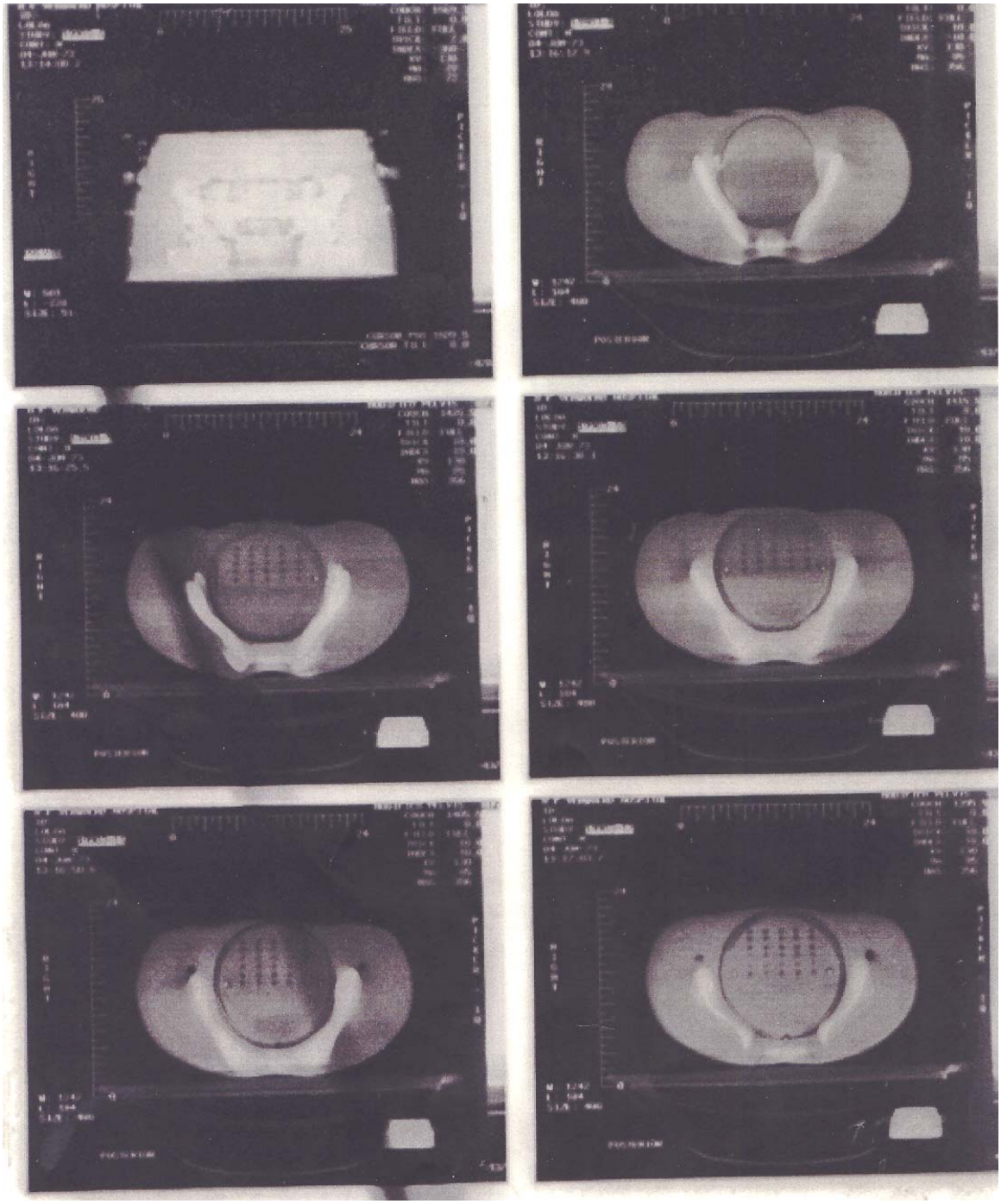

Figure 7 CT therapy module image with TLD positions.

Interest point doses are pre-selected during the treatment planning process and the three treatment modalities as planned are illustrated below (figures 8, 9 and 10). Calculated treatment plans generated by assigning electron densities of 1.70 for bone, and 1.00 for soft tissue and tumour respectively. The treatment plans show the pre-selected interest dose point dose as well as isodose distribution. Selected isodose percentages are All treatments are isocentric with the field size defined at the isocenter.

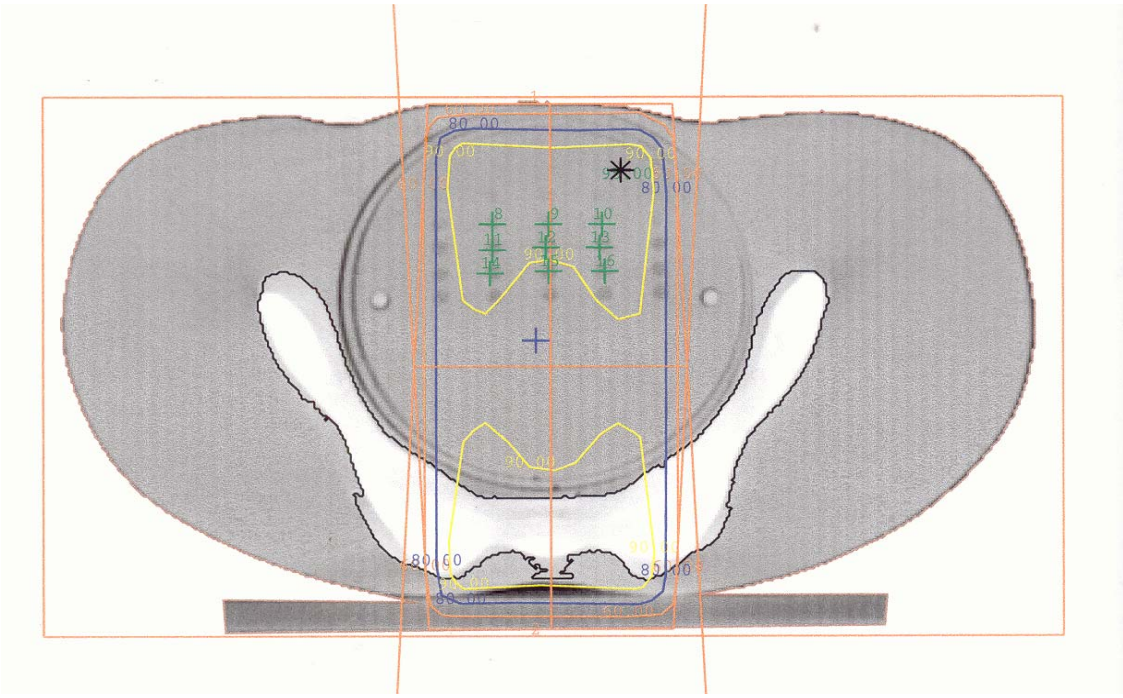

Figure8 Parallel opposed anterior-posterior treatment plan.

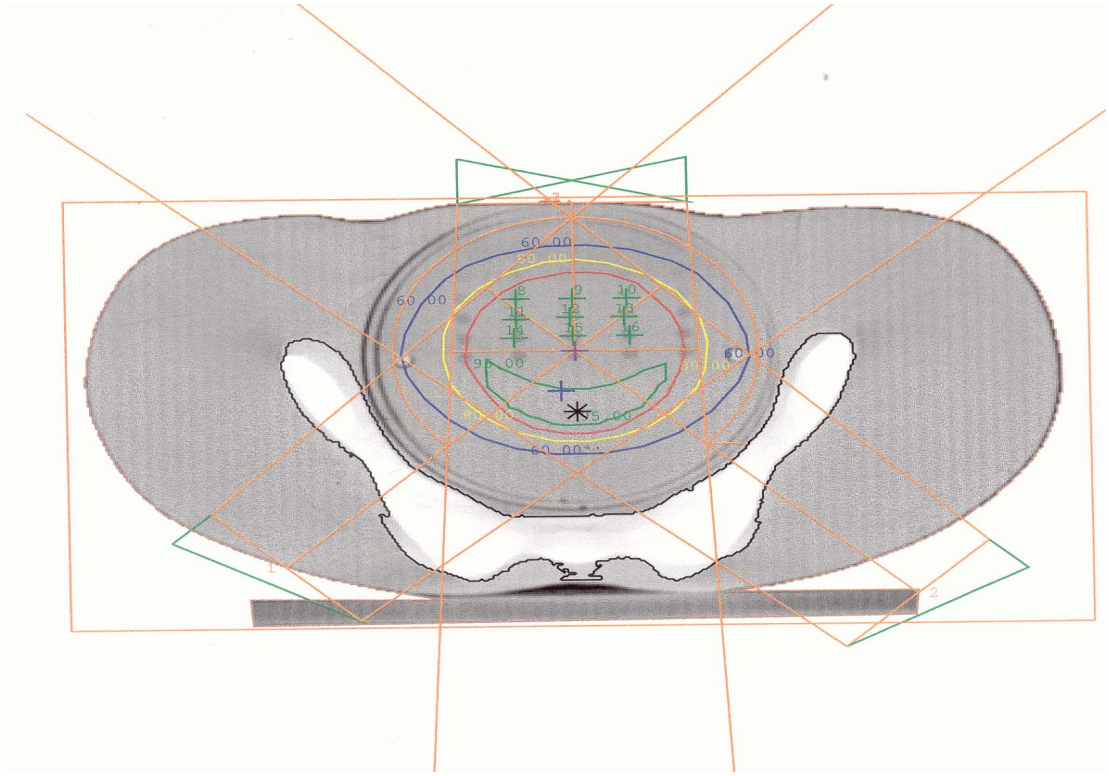

Figure9 Arc therapy treatment plan predicted isodose distribution

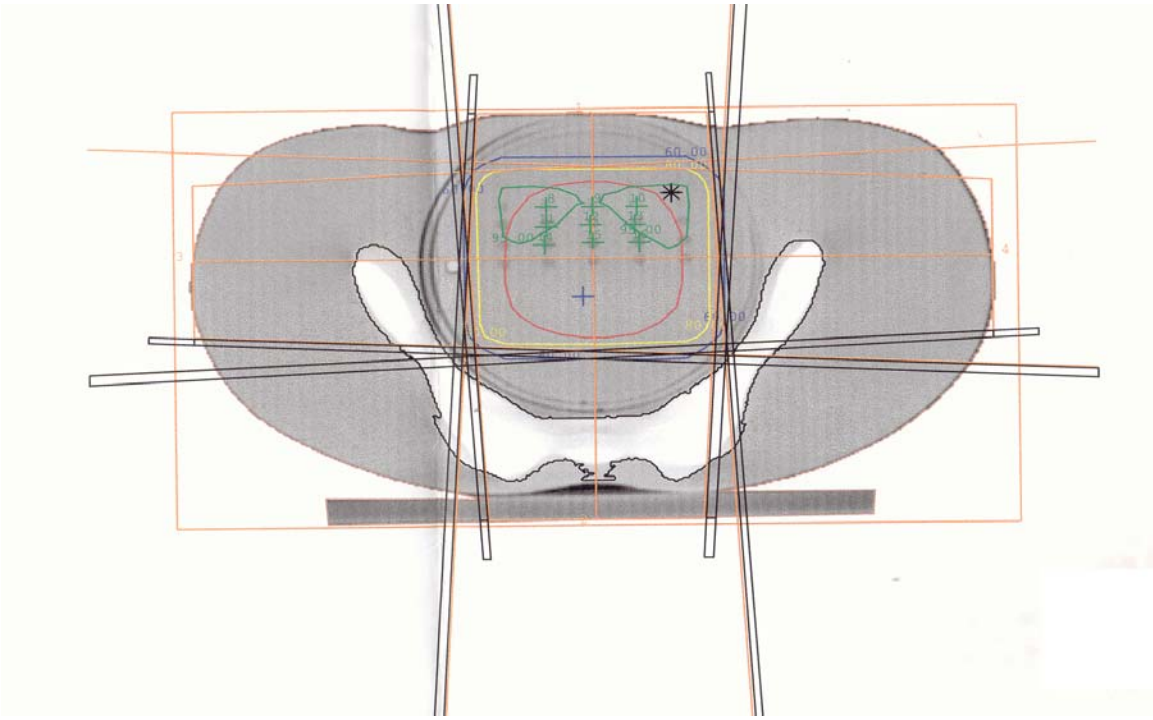

Figure10 Four field treatment plan predicted isodose distribution

4.6.2 Simulation and treatment delivery

Simulation parameters were used to verify the centre of the treatment volume and check for positional alignment with the laser and correct for any errors. All treatment delivery parameters were verified and simulator radiographs showed good positional accuracy. All parameters were well within acceptable limits.

4.6.3 TL dosimetry technique

TLDs dose measurements are compared with treatment planning predicted dose. Figures 11, 12 and 13 show plots of measured dose versus calculated dose for the three treatment modalities. These are absolute doses and normalization of calculated data to measured data has not been done. The predicted dose and measured dose values are separated into high dose and low dose gradient. The high dose gradient regions are those that are in the penumbra region of the radiation field. Each point is an average reading of readings from a single TLD exposed at least twice under the identical conditions for the three treatment modalities. A line of gradient unity is drawn on the graphs. This serves to illustrate the difference in the dose gradients.

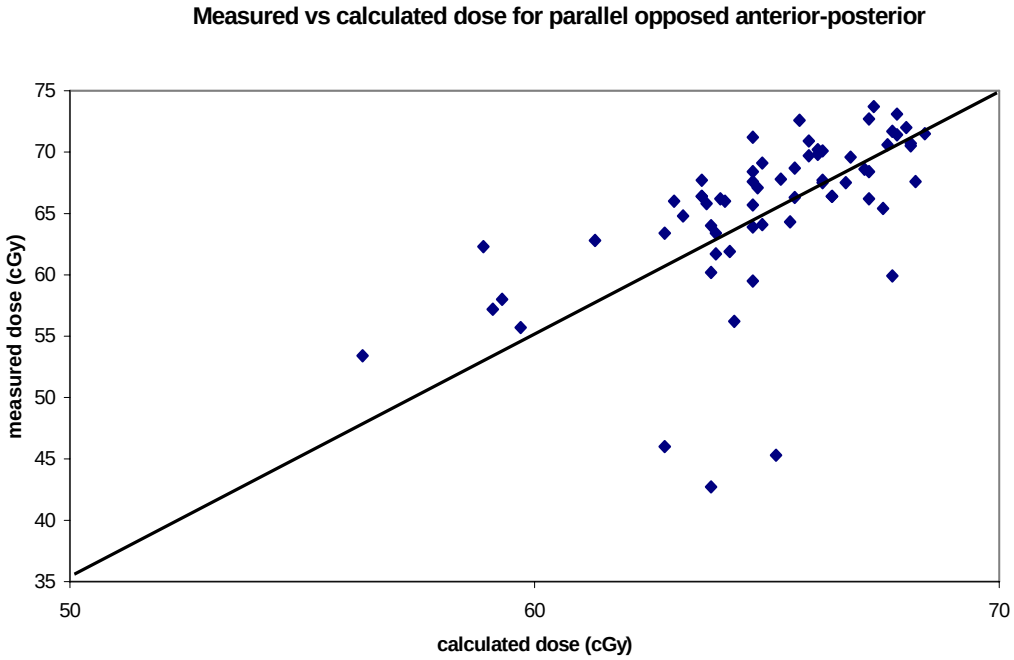

Figure 11 Anterior-Posterior TLD measured against calculated dose

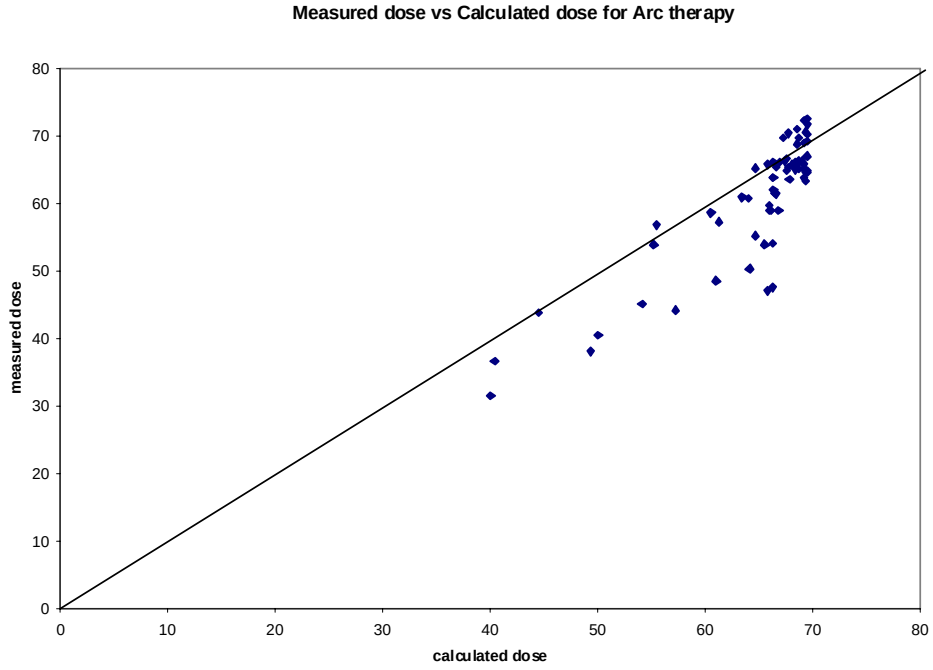

Figure12 Arc therapy TLD measured against calculated dose.

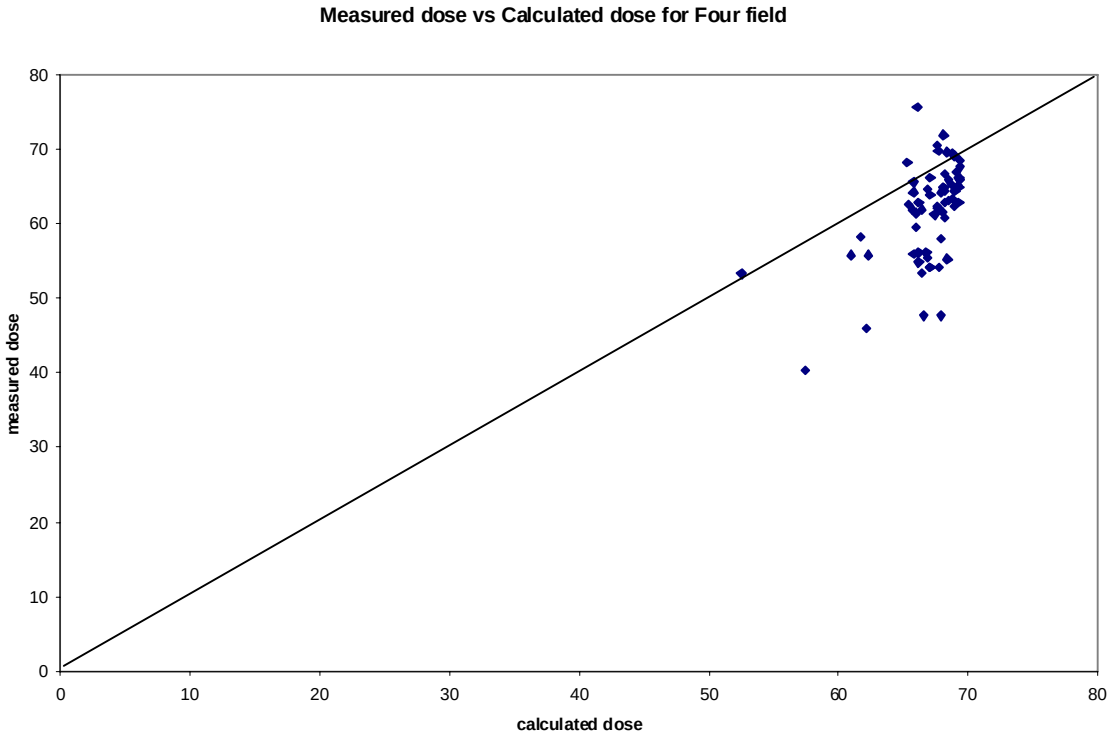

Figure13 Four Field treatment TLD measured against calculated dose.

4.6.4 Film dosimetry technique

Film dosimetry provided a two-dimensional isodose distribution within the irradiated volume. The isodose lines shown are the 98%, 95%, 80%, 60% and 50% as indicated. Figure 14 shows a sample of opposed anterior-posterior treatment film verification, figure 15 shows the four-field treatment film verification and figure 16 shows the arc-therapy treatment film verification.

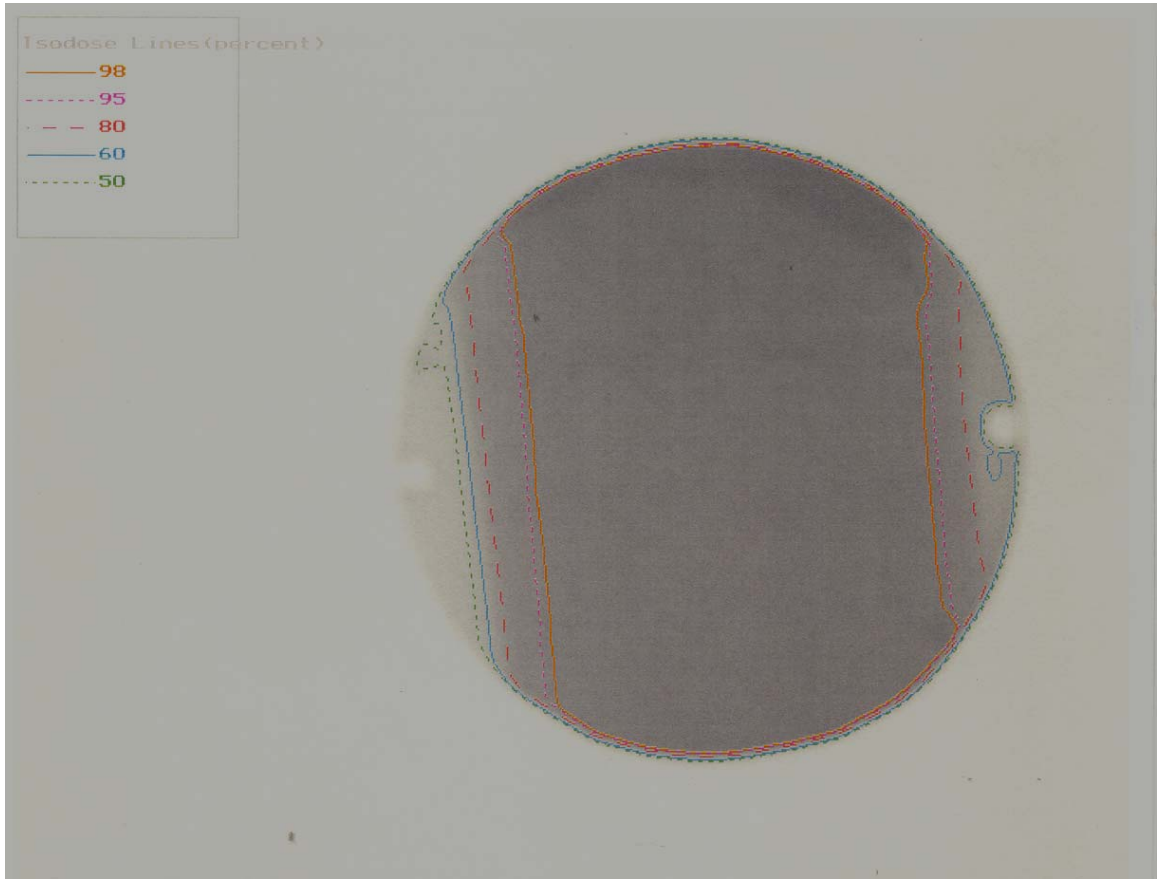

Figure 14B Parallel opposed anterior-posterior film measured isodose distribution.

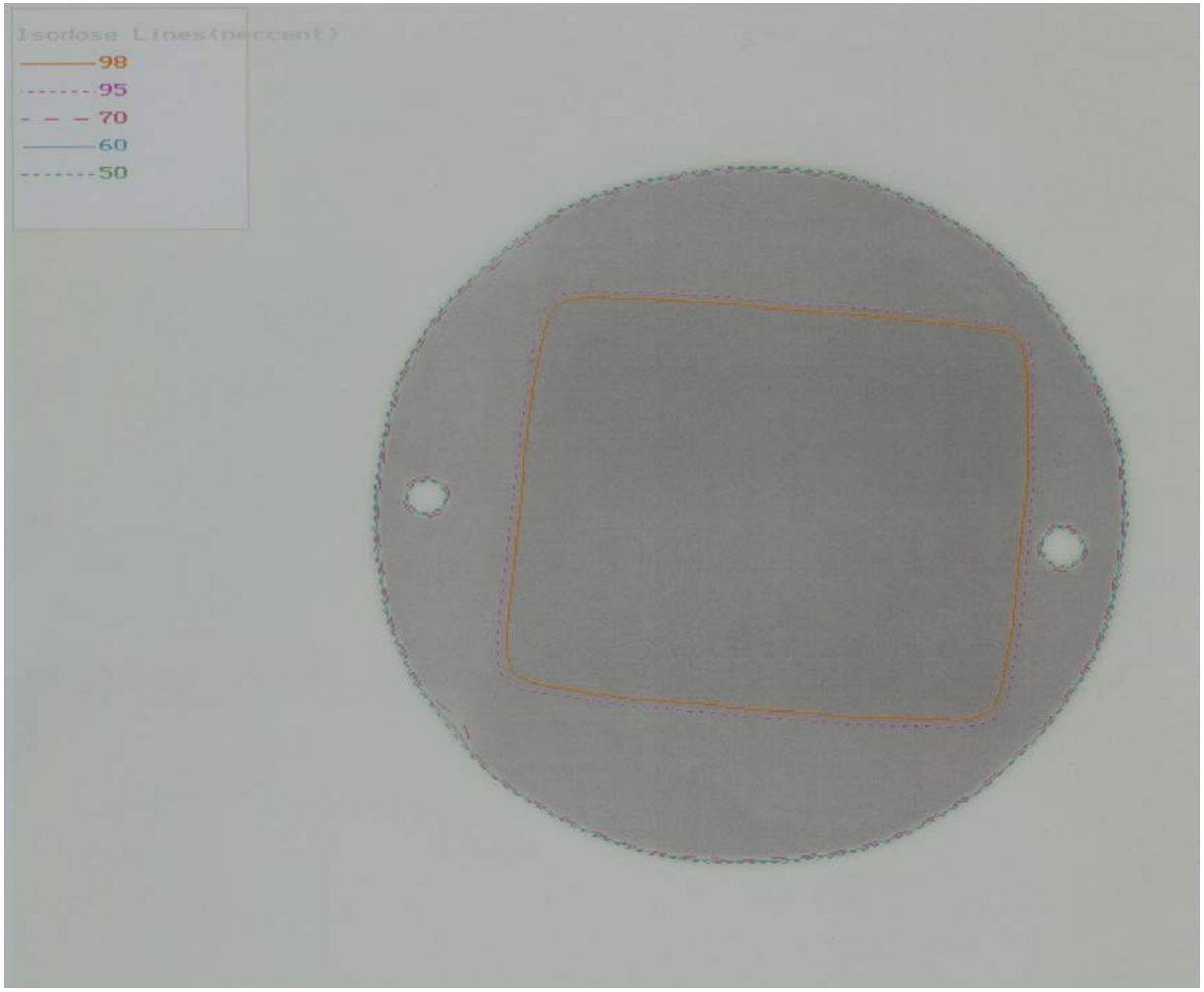

Figure 15 Fourfield film measured isodose distribution.

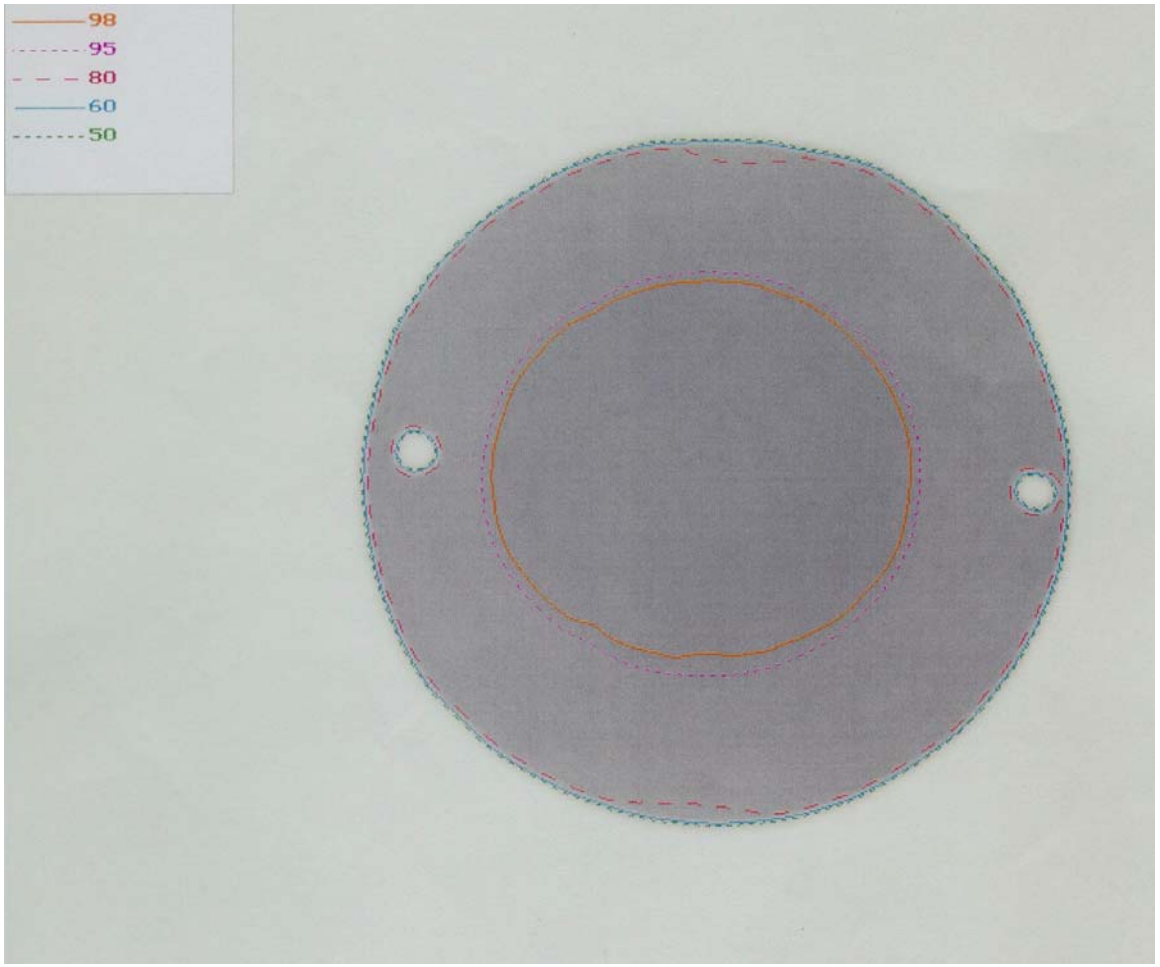

Figure 16 Arc therapy film measured isodose distribution.

5. Discussion

Material Characterization

It is well recognized that the change in the energy spectrum has an influence on the transmission factors defined as the ratio of the energy fluence through different thickness. The reasons for these changes are modifications of the beam penetration and dose deposition with depth in the measuring phantom material. Thus, the atomic number of the phantom material plays a role in the attenuation properties of any material. This is evident in the increase of the effective attenuation coefficient with an increase in atomic number observed across the four materials investigated

The effective attenuation coefficients (μ_{eff}) are calculated for different field sizes and depths in a solid phantom. Results are within ± 3% for different energies measured at the same depth and same field size. The variation across field size is within ± 4%, which indicates that there is a change in μ_{eff} as the field size increases is expected. Variation with energy is also evident and the higher the energy the less attenuation is observed. A plot of the attenuation of the photon beam characteristically follows an exponential curve. The narrow beam effective attenuation coefficient decreases with attenuator thickness. This means there is substantial beam hardening for the lower energy photons.

The intentions of this study, among others, were to find suitable material to simulate a female pelvis. Thus upon characterising the materials investigated with respect to their physical and radiation properties the three materials selected to construct the phantom were easily machinable and readily available. Using aluminium proved to

be difficult both from cost point of view and handling in terms of shaping hence plaster of paris was used as an alternative. The materials used to construct the phantom (plaster of paris, acrylic and dental wax) proved very useful in providing the necessary contrast in terms of density and also in simulating human tissue.

Lightproof testing proved useful as this ensured that film could be placed within the phantom without succumbing to problems such as the film being exposed to ambient light.

Film Dosimetry

The film sensitivity depends on the energy spectrum of the radiation beam. The photon energy spectrum at lager depths shifts towards higher energies (beam hardening) due to greater attenuation of lower energy photons. Hence there is a point at which the optical density of the film saturates and this is why it was desirable to determine the dose limit by calibration. Beyond ±80 monitor units (equivalent to 80cGy at d_{max}) it was observed that the film does not provide any dosimetrical information because the optical density is uniform. Film calibration provided a means to quantify this effect. Film response is determined as a function depth for a fixed field size and is reported in terms of optical density versus dose from which a dose calibration or H-D curve is determined. The general trend is that the optical density will decrease with depth due to the low-energy scattered radiation. Calibration film was used to process the treatment verification film by the densitometer software.

TL dosimetry

Thermoluminescent sensitivity, which is defined as the integrated signal from the PMT per unit of radiation exposure, depends on the characteristics of the TLDs and of the TLD reader system. The response curve of the TLDs used was linear over the full useful exposure range for ease of calibration and use. Background subtraction correction was performed for each TLD. TL output per unit dose was independent of dose up to 100cGy. Any discrepancies indicate a poor response per unit dose of the individual TLD and systematic factors such as background subtraction being overcorrected and the uncertain effect of the observed existence of small residual signal after readout. On the whole, most of the TLDs used performed well within acceptable limits of ±5% and disparities of up to 28% were observed.

Treatment validation

CT scan images allowed for the possibility to assign interest dose points within the localized tumour volume. The well-constructed radiographs attribute to not only to proper imaging of the phantom but also the difference in the material used to fabricate the phantom in terms of the radiological and radiation properties. Images both from CT and simulator show good contrast hence the materials selected were suitable from a diagnostic perspective.

The irradiated volume is larger than the treatment volume and receives a dose significant in relation to tissue tolerance. This brings in the aspect of the rectum, which inherently receives a dose by virtue of being in the path of the beam. The rectum is well within the 95% isodose level for the anterior-posterior and four-field

treatment modalities. The arc treatment spares the rectum reasonably well from the high dose levels (> 50%).

Film dosimetry was used as check for spatial dose distribution and positional verification of predicted target by the planning system. Film was used to determine a two-dimensional isodose distribution of the dose delivered within the target volume. A comparison for predicted and measured isodose distribution reveals good distance agreement. As a quality measure, the isodose lines follow the same general trend for both the predicted and measured isodose distribution. Quantitatively, positional discrepancies of the data generated from the scanning densitometer compared with the predicted isodose distribution were within ±5mm. The disparity observed between the measured dose distribution from the film and the predicted dose distribution can be attributed to the calculations failure to incorporate scatter into the calculations.

TL dosimetry provided the other treatment validation criteria for the three treatment methods. Observation of the measured-calculated dose curves, it is apparent that they are a number of discrepancies and ideally all the points should lie along the unity line. The lager the discrepancy, the further the point is away from this line. This is attributed to the high dose gradient (penumbra) region of a radiation field.

The discrepancies observed in the TLD measured dose can be attributed to inherent uncertainties in the TLD chips used. This was accounted for by the reader correction factor and the ECC of each TLD chip. In as much as this is so, there still is the loss in sensitivity of the TLD chip over time and with frequent use. Further uncertainties are a result of possible positional movements and beam output fluctuations. It was

observed that repeated use resulted in a drop of about 1.5-2% of the initial reading, an indication of the fading sensitivity inherent in most TLD materials.

The maximum level of the interest point dose is within the linear region of the TLD sensitivity. TLDs were calibrated for dose readings up to 70 cGy, which is well above the maximum prescribed dose in the target volume. The TLDs have served well as point dose measuring devices. It is observed that TLDs places at low dose gradient regions have lower discrepancies than those at the peripheral high dose gradient regions. This is due the steep drop in dose levels at the field edge of a beam. Also, the readings are an average of two readings measured on different days.

6. CONCLUSIONS and RECOMMENDATIONS

This study investigated the feasibility and utility of a phantom designed to verify the radiotherapy process. It has shown that the treatment delivery at Pretoria Academic Hospital is accurate within the limits tested by the system. Further, it has demonstrated the implementation of a dosimetric verification system to check the correspondence between predicted and measured dose as well as predicted dose distribution and measured dose distribution.

Absolute dose values at interest points located in the target volume within the phantom have been verified with TLDs placed in the phantom during treatment delivery. These measurements were within the pre-selected acceptable difference of ±5%. Larger discrepancies were also observed and attributed to inherent uncertainties of the TLDs and position within target area. Isodose distributions have been determined by radiographic films and compared with those predicted by the planning system. Distance to agreement between predicted and measured isodoses was within ±5mm. The results indicate that the phantom serves well its purpose of treatment delivery verification.

The dosimetric techniques developed are characterized by reproducibility, reliability and accuracy of the radiation dose measurements. Thus, the techniques are quantitatively and qualitatively practical. The measurements and analysis demonstrate that the phantom and measuring tools were sufficient and useful for the treatments applied.

The materials used to construct the phantom are low cost and are readily available in most radiotherapy departments. Fabrication of the phantom was done carefully so as to incorporate dosimetry aspects, anatomical simulation as well as diagnostic and therapeutic radiation properties.

RECOMMENDATIONS:

1. Investigation of other materials to be used to simulate various sections of the human body.
2. Provide for ionisation chamber measurements.
3. Improve on accuracy of CT scanning by providing markers within the phantom to ensure accurate positioning.
4. Practical aspects such as increasing packing space of film in phantom so as to provide more room for a number of films to be stacked at once so as to save on time.

APPENDIX A

A.1 Physical constants

1 atomic mass unit (amu) = 1.66 x 10^{-27} kg A1

Avogadro's number (N_A) = 6.0225 x 10^{23} mol^{-1} A2

A.2 Physical Properties

The physical density of the materials was calculated by direct measurement using the formula :

Density = mass / volume A3

Where the volume is calculated by

Volume = length (l) x breadth (b) x height (h) A4

APPENDIX B

B.1 Electron density

The electron density, ρ_e is calculated form the equation

$$\rho_e = \rho_m N_A \left(\frac{Z}{A}\right) \quad \text{B1}$$

where

$$\frac{Z}{A}\sum a_i \left(\frac{Z_i}{A_i}\right)$$

N_A is avogadro's number and a_i is the fraction by weight of the ith element of atomic number Z_i and atomic weight A_i. ρ_m is the the physical density of the material of interest.

B.2 Effective Atomic Number Z_{eff} of a compound

Effective atomic number is calculated from the equation

$$Z_{eff} = \left[a_1 Z_1^m + a_2 Z_2^m + ... + a_n Z_n^m\right]^{1/m} \qquad \text{B2}$$

Where $a_1, a_2, \ldots a_n$ are the fractional contributions of each element to the total number of electrons in the mixture; $Z_1, Z_2, \ldots Z_n$ are the atomic numbers of elements in the compound, and m is an integer dependent on the mode of interaction of x-rays with matter [20,21]. Since photoelectric effect is highly dependent on atomic number, the effective atomic number is calculated from equation B2 above for $m = 2.94$. a reasonable approximation for Z_{eff} can be computed for $m = 3$. The effective atomic number of a material is the atomic number of a hypothetical single element that attenuates photons at the same rate as the material.

APPENDIX C

C.1 Calculation of attenuation coefficients.

Let N_0 be the number of incident photons per unit area. Considering a thickness of Δx of attenuator material, then for N_0 photons incident on the surface, ($N_0 - dN$) will exit as some will be scattered from the beam.

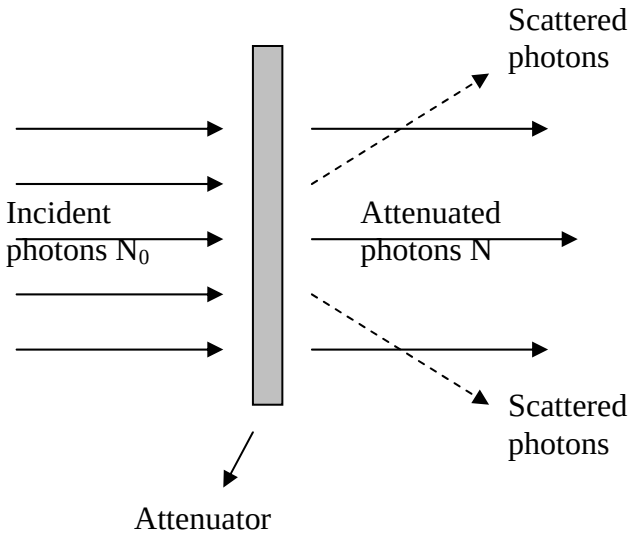

Figure C.1 diagram to illustrate how an attenuator of thickness Δx reduces the number of incident photons from N_0 to N.

The loss dN is proportional to

(i) the number of incident photons N_0, and

(ii) the thickness dx

Thus we have

$$dN = -\mu N dx \qquad \text{C1}$$

where μ is the proportionality constant. The negative sign indicates a reduction.

C.2 Linear Attenuation Coefficient

μ is called the linear attenuation coefficient and has dimensions of the reciprocal of length (cm^{-1}).

The attenuation has an exponential behaviour obtained by integrating equation C1. Thus we have

$$\int_{N_0}^{N} \frac{dN}{N} = \int_{0}^{x} -\mu\, dx \qquad \text{C2}$$

then,

$$\frac{N}{N_0} = e^{-\mu x} \qquad \text{C3}$$

The factor $\frac{N}{N_0}$ is called the transmission factor which is the ratio of the exit intensity N to the entrance intensity N_0.

The linear attenuation coefficient is obtained from the equation

$$\mu = -\frac{1}{x}\ln\left(\frac{N}{N_0}\right) \qquad \text{C4}$$

x is in centimeters and μ is in cm^{-1}.

C.3 Mass Attenuation Coefficient

It is ideal use an attenuation coefficient that is independent of the state of matter of the attenuator material. Therefore the mass attenuation coefficient removes the dependence on the state of matter of the material by dividing by the density of the material of interest. Thus we have the mass attenuation coefficient given as

$$\frac{\mu}{\rho} = -\frac{1}{x}\ln\left(\frac{N}{N_0}\right) \qquad \text{C5}$$

where ρ is the physical density. The units of the mass attenuation coefficient are $cm^2.g^{-1}$.

APPENDIX D

D.1 Physical Density calculations

material	**Mass**	**Volume = *Length x breadth x height***	**Density =** $\frac{mass}{volume}$
Wax			
(i) 5 sheets	(i) 100 g	18.92cm x 8.88cm x 0.8cm = 134.41 cm^3	0.74 $g.cm^{-3}$
(ii) 32 sheets	(ii) 750 g	18.92cm x 8.88cm x 5.0cm = 840.05cm^3	0.89 $g.cm^{-3}$
			D_{av}= 0.816 $g.cm^{-3}$
Perspex			
1 sheet	550g	25.5cm x 31cm x 0.6cm = 474.3 cm^3	1.16 $g.cm^{-3}$

material	**Mass**	**Volume = length x breadth x height**	**Density (ρ_m) = $\frac{mass}{volume}$**
Plaster of Paris			
Block 1	850g	22.6cm x 22.2cm x1.25cm=627.15cm^3	1.35 g.cm^{-3}
Block 2	2250g	22.6cm x 22.2cm x 3.17cm=1555.33cm^3	1.45 g.cm^{-3}
Block 3	3000g	22.6cm x 22.2cm x4.04cm = 2023.95	1.48 g.cm^{-3}
Block 4	4700g	22.6cm x 22.2cm x 6.30cm=3160.84cm^3	1.49 g.cm^{-3}
			D_{av} = 1.43 g.cm^{-3}

D.2 Calculation of Mass Percentage Composition

The following equations are used:

(i) *Molar Mass of a Compound* = sum of molar mass of constituents

(ii) *Number of moles* = $\frac{\text{mass of sample (1g)}}{\text{Molar mass (g . mol}^{-1})}$

(iii) *Mass of each element in sample* = number of moles x molar mass of element

(iv) *mass percentage of element* = $\frac{\text{mass of element in 1g of sample}}{\text{total mass of sample}}$ x 100

Material	Molar mass of compound	Number of moles in compound	Mass percentage of each element (%)
*Wax (C_nH_{2n+2})	*	*	*C: 14.86 H: 85.14
Perspex ($C_5H_4O_2$)	(5x12.01) + (4x1.0079) + (2x16) = 96.0816 $g.mol^{-1}$	$\frac{1g}{96.0816g.mol^{-1}} = 0.01mols$	C: 62.45 H: 33.28 O: 1.5
Aluminium (Al)	100	-	100
Plaster of paris ($CaSO_4{:}2H_2O$)	40.08 +32.06 + (6x16) + (4x1.0079) = 136.14 $g.mol^{-1}$	$\frac{1g}{172.1716g.mol^{-1}} = 0.0058mols$	Ca: 23.27 S: 18.62 O: 55.75 H: 2.34

* dental wax used is a combination of various waxes therefore the general formula is used here. Mass percentages are obtained form consultation and internet searches.

D.3 Calculations for Effective Atomic Number Z_{eff}

Z_{eff} is calculated form the equation

$$Z_{eff} = \left[a_1 Z_1^m + a_2 Z_2^m + ...+ a_n Z_n^m\right]^{1/m}$$

where m=2.94.

Number of electrons per 1 gram of material = $\frac{w_i N_A Z_i}{A_i}$

(i) Z_{eff} for Wax (C_nH_{2n+2})

Carbon: $\frac{0.1486 \times (6.022 \times 10^{23}) \times 6}{12.01} = 4.47 \times 10^{22} electrons$

Hydrogen: $\frac{0.8514 \times (6.022 \times 10^{23}) \times 1}{1.0079} = 5.08 \times 10^{23} electrons$

Total number of electrons = 5.53 x 10^{23}

Fractional contribution of electrons:

$$\alpha_C = \frac{4.47 \times 10^{22}}{5.53 \times 10^{23}} = 0.081$$

$$\alpha_H = \frac{5.08\times10^{22}}{5.53\times10^{23}} = 0.92$$

$$Z_{eff} = \left[\alpha_C Z_C^{2.94} + \alpha_H Z_H^{2.94}\right]^{1/2.94}$$

$$= \left[\left(0.081\times6^{2.94}\right) + \left(0.92\times1^{2.94}\right)\right]^{1/2.94}$$

= 2.60

(ii) Z_{eff} for Perspex ($C_5H_4O_2$)

Carbon: $\frac{0.625\times(6.022\times10^{23})\times6}{12.01} = 1.88\times10^{23}\,electrons$

Oxygen: $\frac{0.333\times(6.022\times10^{23})\times8}{16} = 1.002\times10^{23}\,electrons$

Hydrogen: $\frac{0.015\times(6.022\times10^{23})\times1}{1.0079} = 8.96\times10^{21}\,electrons$

Total number of electrons = 2.97 x 10^{23}

Fractional contributions of electrons:

$$\alpha_C = \frac{1.88\times10^{23}}{2.97\times10^{23}} = 0.633$$

$$\alpha_O = \frac{1.002\times10^{23}}{2.97\times10^{23}} = 0.337$$

$$\alpha_H = \frac{8.96\times10^{21}}{2.97\times10^{23}} = 0.030$$

$$Z_{eff} = \left[\alpha_C Z_C^{2.94} + \alpha_O Z_O^{2.94} + \alpha_H Z_H^{2.94}\right]^{1/2.94}$$

$$= \left[\left(0.633 \times 6^{2.94}\right) + \left(0.337 \times 8^{2.94}\right) + \left(0.030 \times 1^{2.94}\right)\right]^{1/2.94}$$

$$= 6.75$$

(iii) Z_{eff} for Plaster of Paris ($CaSO_4{:}2H_2O$)

Number of electrons contributed to 1 gram of P.O.P:

Calcium: $\frac{0.2327 \times (6.022 \times 10^{23}) \times 20}{40.08} = 6.99 \times 10^{22}\ electrons$

Sulfur: $\frac{0.1862 \times (6.022 \times 10^{23}) \times 16}{32.06} = 5.59 \times 10^{22}\ electrons$

Oxygen: $\frac{0.5575 \times (6.022 \times 10^{23}) \times 8}{16} = 1.67 \times 10^{23}\ electrons$

Hydrogen: $\frac{0.0234 \times (6.022 \times 10^{23}) \times 1}{1.0079} = 1.39 \times 10^{22}\ electrons$

Total number of electrons = 3.07×10^{23}

Fractional contribution of electrons:

$$\alpha_{Ca} = \frac{6.99 \times 10^{22}}{3.07 \times 10^{23}} = 0.228$$

$$\alpha_S = \frac{5.59 \times 10^{22}}{3.07 \times 10^{23}} = 0.182$$

$$\alpha_O = \frac{1.67 \times 10^{23}}{3.07 \times 10^{23}} = 0.544$$

$$\alpha_H = \frac{1.39 \times 10^{22}}{3.07 \times 10^{23}} = 0.044$$

$$Z_{eff} = \left[\alpha_{Ca} Z_{Ca}^{2.94} + \alpha_S Z_S^{2.94} + \alpha_O Z_O^{2.94} + \alpha_H Z_H^{2.94}\right]^{1/2.94}$$

$$= \left[\left(0.228 \times 20^{2.94}\right) + \left(0.182 \times 16^{2.94}\right) + \left(0.544 \times 8^{2.94}\right) + \left(0.044 \times 1^{2.94}\right)\right]^{1/2.94}$$

$$= 14.11$$

D.4 Calculation Of Electron Density

Calculations are based on the equation

$$\rho_e = \rho_m N_A \left(\frac{Z}{A}\right)$$

material	$\rho_m N_A$	$\frac{Z}{A} = \sum a_i \left(\frac{Z_i}{A_i}\right)$	**Eletron density ρ_e (electrons/g)**
Wax	4.91 x 10^{23}	0.953	4.68 x 10^{23}
Perspex	6.98 x 10^{23}	0.514	3.59 x 10^{23}
Plaster of paris	8.61 x 10^{23}	0.520	4.47 x 10^{23}
Aluminium	*	*	2.902 x 10^{26}

***** aluminium is a pure substance.

D.5 Calculation of Attenuation Coefficients

Calculation of the linear attenuation coefficients derived from the equation

$$\mu = -\frac{1}{x} \ln\left(\frac{N}{N_0}\right)$$

and the mass attenuation coefficient is calculated from the equation

$$\frac{\mu}{\rho_m} = -\frac{1}{x} \ln\left(\frac{N}{N_0}\right)$$

where ρ_m is the material density.

ACRYLIC						
Field size	2cm x 2cm		4cm x 4cm		6cm x 6cm	
Energy	μ	μ/ρ	μ	μ/ρ	μ	μ/ρ
6MV: d_1	0.055	0.047	0.055	0.047	0.055	0.047
d_2	0.051	0.044	0.053	0.045	0.052	0.045
10MV: d_1	0.044	0.038	0.044	0.038	0.043	0.037
d_2	0.029	0.025	0.041	0.035	0.038	0.033

ALUMINIUM						
Field size	2cm x 2cm		4cm x 4cm		5cm x 5cm	
Energy	μ	μ/ρ	μ	μ/ρ	μ	μ/ρ
8MV	0.010	0.03	0.009	0.03	0.012	0.04

PLASTER OF PARIS						
Field size	2cm x 2cm		4cm x 4cm		6cm x 6cm	
Energy	μ	μ/ρ	μ	μ/ρ	μ	μ/ρ
6MV: d_1	0.083	0.058	0.083	0.058	0.083	0.058
d_2	0.068	0.047	0.068	0.047	0.075	0.052
10MV: d_1	0.075	0.052	0.075	0.052	0.068	0.048
d_2	0.062	0.043	0.062	0.043	0.066	0.046

WAX						
Field size	2cm x 2cm		4cm x 4cm		6cm x 6cm	
Energy	μ	μ/ρ	μ	μ/ρ	μ	μ/ρ
6MV: d_1	0.044	0.054	0.057	0.044	0.044	0.054
d_2	0.041	0.050	0.055	0.047	0.047	0.057
10MV: d_1	0.036	0.044	0.025	0.031	0.034	0.042
d_2	0.033	0.040	0.052	0.064	0.035	0.043

APPENDIX E

ANTERIOR-POSTERIOR INTEREST DOSE POINTS

calculated dose	measured dose	**Percentage difference**
68.1	69.5	**-2.1**
68.2	67.2	**1.5**
67.6	68.8	**-1.8**
67.7	71.1	**-5.9**
67.2	73	***-8.6**
67.2	65.6	**2.4**
67.8	75	***-10.6**
67.8	70.7	**-4.3**
67.2	67.3	**-0.2**
67.1	68.2	**-1.6**
68.1	69.3	**-1.8**
68.0	71.3	**-4.9**
67.8	69.6	**-2.6**
68.4	70.5	**-3.1**
65.7	70.3	***-7.0**
65.9	68.1	**-3.3**
65.9	70.1	***-6.4**
66.2	67.5	**-1.9**
66.8	67.5	**-1.1**
66.4	64.9	**2.3**
66.2	67.7	**-2.3**
67.3	69.4	**-3.1**
64.9	67.4	**-3.9**
64.8	65.8	**-1.5**
64.7	67.6	**-4.5**
65.3	67.0	**-2.6**
66.4	67	**-0.9**
66.3	66.4	**-0.2**
64.7	68.2	***-5.4**
64.2	66.7	**-3.9**
63.6	66.3	**-4.2**
63.9	64.7	**-1.3**
63.8	64.3	**-0.8**
64.7	67.1	**-3.7**
63.7	64.5	**-1.3**
64.7	65.6	**-1.4**
64.1	64.8	**-1.1**
63.2	62.9	**0.5**
64.0	65.9	**-2.9**
63.6	66.4	**-4.4**
62.8	64.5	**-2.7**
63.6	63.9	**-0.5**
61.3	62.5	**-1.9**
65.2	51.3	***21.3**
59.7	56.6	**5.2**
63.9	63.4	**0.8**
63.8	46.9	**26**
59.3	57.8	**2.5**
62.8	46.0	***26.8**
58.9	62.3	**-5.8**
65.5	64.3	**1.8**
64.7	59.5	***8.0**
59.1	57.2	**3.2**
63.8	60.2	***5.6**
67.7	59.4	***12.3**
67.5	65.4	**3.1**
56.3	53.4	***5.2**
65.6	66.3	**-1.1**
64.3	56.2	***12.6**
64.9	64.1	**1.2**
64.7	63.9	**1.2**
66.7	67.5	**-1.2**
66.2	70.1	***-5.9**
66.1	70.2	***-6.2**
66.1	69.8	***-5.6**
65.6	68.7	**-4.7**

***** **I**ndicates regions of high dose gradient.

ARC THERAPY INTEREST DOSE POINTS

calculated dose	measured dose	percentage difference
69.4	67.1	**3.3**
69.3	63.4	***8.5**
69.4	64.7	***6.8**
69.4	69.3	**0.1**
69.5	70.4	**-1.3**
69.5	64.9	***6.6**
69.1	65.9	**4.6**
69.0	66.3	**3.9**
69.1	63.8	***7.7**
69.1	65.3	**5.5**
63.4	61.0	**3.8**
68.1	65.8	**3.4**
68.3	65.1	**4.7**
64.6	55.3	***14.4**
69.1	69.1	**0.0**
68.5	71.1	**-3.8**
68.4	66.2	**3.2**
69.1	65.1	***5.8**
64.0	60.8	***5.0**
67.4	66.4	**1.5**
67.5	64.9	**3.9**
65.5	54.0	***17.6**
68.7	66.5	**3.2**
67.8	63.7	**6.0**
67.7	65.4	**3.4**
68.6	65.2	**5.0**
61.2	57.3	**6.4**
64.1	50.4	***21.4**
66.3	66.2	**0.2**
66.3	63.9	**3.6**
66.2	63.9	**3.5**
67.2	69.8	**-3.9**
66.9	66.2	**1.0**
66.2	54.2	***18.1**
66.0	59.1	***10.5**
66.2	47.6	***28.1**
66.4	61.7	***7.1**
65.9	59.8	***9.3**
66.3	62.1	***6.3**
66.6	65.5	**1.7**
65.8	65.9	**-0.2**
66.5	61.5	***7.5**
40.4	36.7	***9.2**
40.0	31.6	***21.0**
55.2	54.0	**2.2**
66.1	59.0	***10.7**
57.2	44.2	***22.7**
64.6	65.3	**-1.1**
67.5	66.7	**1.2**
44.5	43.8	**1.6**
49.3	38.1	***22.7**
66.8	59.0	**11.7**
60.5	58.7	**3.0**
65.8	47.1	***28.4**
50.0	40.5	***19.0**
54.1	45.1	***16.6**
55.4	56.9	**-2.7**
67.7	70.5	**-4.1**
61.0	48.6	***20.3**
68.7	66.1	**3.8**
68.5	68.9	**-0.6**
68.7	69.9	**-1.7**
69.4	72.6	**-4.6**
69.1	72.4	**-4.8**
69.3	70.7	**-2.0**
69.5	71.8	**-3.3**

***** Indicates regions of high dose gradient.

Four-field Interest dose points

calculated dose	measured dose	Percentage difference
69.3	64.9	***6.35**
69.3	62.9	***9.24**
69.0	64.5	***6.52**
69.1	66.9	**3.18**
68.8	69.4	**-0.87**
68.8	65.1	**5.38**
69.4	66	**4.90**
69.4	65.9	**5.04**
69.1	62.9	***8.97**
69.0	69.1	**-0.14**
67.1	63.8	**4.92**
67.1	66.2	**1.34**
68.1	64.8	**4.85**
68.5	65.8	**3.94**
68.4	55.3	***19.15**
68.1	71.9	**-5.58**
68.1	64.9	**4.70**
68.5	63.1	**7.88**
68.2	60.8	***10.85**
67.4	61.2	***9.20**
68.0	61.6	***9.41**
68.9	62.4	***9.43**
68.2	62.8	***7.92**
67.7	62.1	***8.27**
67.6	62.4	***7.69**
68.2	66.7	**2.20**
61.7	58.3	**5.51**
61.0	55.8	***8.52**
65.8	64.2	**2.43**
66.1	75.6	***-14.37**
65.7	61.9	**5.78**
65.8	65.6	**0.30**
68.8	63.4	**7.85**
66.9	64.6	**3.44**
66.2	54.8	***17.22**
66.9	55.4	***17.19**
66.4	53.4	***19.58**
65.8	56	***14.89**
66.4	61.9	***6.78**
66.0	61.4	***6.97**
65.4	62.6	**4.28**
66.0	59.5	***9.85**
57.4	40.4	***29.62**
52.5	53.3	**-1.52**
66.2	62.9	**4.98**
67.9	47.7	***29.75**
67.1	54.2	***19.23**
66.2	56.1	***15.26**
67.9	64.2	**5.45**
67.1	54.1	***19.37**
66.6	47.7	***28.38**
67.8	54.2	***20.06**
66.8	56.1	***16.02**
67.9	58	***14.58**
62.3	55.8	***10.43**
62.2	45.9	***26.21**
65.3	68.2	**-4.44**
68.4	69.6	**-1.75**
68.2	64.5	**5.43**
67.6	70.6	**-4.44**
67.7	69.7	**-2.95**
69.4	68.5	**1.30**
69.4	67.6	**2.59**
69.2	65.2	**5.78**
69.3	66.1	**4.62**
68.9	64.4	***6.53**

***** Indicates regions of high dose gradient.

REFERENCES

1. Swinnen A. et al, *The Use Of A Multipurpose Phantom For Mailed Dosimetry Checks Of Therapeutic Photon Beams: "Opera" (Operational Phantom For External Radiotherapy Audit)*, Radiotherapy & Oncology, 64, 317-326,2002.
2. Ferguson H.M. et al, *Automated TLD System For Tumor Dose Estimation From Exit Dose Measurements In External Beam Radiotherapy*, Int. J. Radiation Oncology Biol. Phys., 38, 899-905,1997.
3. Calandrino R. et al, *Detection Of Systematic Errors In External Radiotherapy Before Treatment Delivery*, Radiotherapy & Oncology, 45, 271-274, 1997,
4. *International Commission On Radiation Units And Measurements Determination Of Absorbed Dose In A Patient Irradiated With Beams Of X Or Gamma Rays In Radiotherapy Procedures. Report 24*, ICRU, Washington, 1976.
5. Perrin B.A. et al, *The Design And Evaluation Of A Phantom For The Audit Of Treatment Chain For Prostate Radiotherapy*, Radiotherapy and Oncology, 60(1), 37-43, 2001.
6. Paliwal B.R. et al, *A Solid Water Pelvic And Prostate Phantom For Imaging, Volume Rendering, Treatment Planning, And Dosimetry For An RTOG Multi-Institutional, 3-D Dose Escalation Study*, Int. J. Radiation Oncology Biol. Phys., 42,205-211,1998.
7. Fallone B.G. et al, *Verification Of The Correspondence Between CT-Simulated And Treatment Beams*, Med. Phys. 25(5), 351-355, 2002.
8. Mayer R. et al, *Two dimesional film dosimetry in heterogenous materials exposed to megavoltage photon beams*, Med. Phys. 24(3), 455-460, 1997.
9. Leybovich L.B. et al, *Comparison of ionization chambers of various volumes for IMRT absolute dose verification*, Med. Phys., 30(2), 119-123, 2003.
10. Yu C. and Luxton G., *TLD dose measurements: A amplified accurate technique for the dose range from 0.5 cGy to 1000 cGy*, Med. Phys. 26(6), 1010- 6, 1999.
11. Takahiko A. et al, *An in-phantom dosimetry system using pin silicon photodiode radiation sensors for measuring organ doses in x-ray CT and other diagnostic radiology*, Med. Phys. 29 (7), 1505-1510, 2002.

12. Van Dyk J., *The Modern Technology of Radiation Oncology, A Compendium for Medical Physicist and Oncologists*, Medical Physics Publishing, Wisconsin, 1999.
13. Huq M.S. et al, *Comparison Of The IAEA TRS-389 And AAPM TG-51 Absorbed Dose To Water Protocols In The Dosimetry Of High –Energy Photon And Electron Beams*, Phys Med Biol, 46(11), 2985 –3006,2001.
14. Stewart K.J. et al, *Comparing Calibration Methods Of Electron Beams Using Plane –Parallel Chambers With Absorbed –Dose To Water Based Protocols*, Med Phys, 29(2), 2001,
15. Banjade D.P. et al, *Determination Of Absorbed Dose For Photon Beams And Electron Beams From A Linear Accelerator By Comparing Various Protocols On Different Phantoms*, Applied Radiation and Isotopes, 55, 235 –243,2001.
16. Danciu C. et al, *Variation Of Sensitometric Curves Of Radiographic Films In High Energy Photon Beams*, Med Phys 28(6), 2001.
17. Bentel G.C, *Radiation Therapy Planning*, Mcgraw-Hill-inc, 1991.
18. Bentel G.C. et al, *Treatment Planning And Dose Calculation In Radiation Oncology Fourth Edition*, Peragon Press, 1989.
19. Jayaraman S. and Hanzl L.H., *Clinical Radiotherapy Physics: Basic Physics and Dosimetry, Volume 1*, CRC Press, 1996.
20. Hendee W.R. and Ibbot G.S., *Radiation Therapy Physics, Second Edition*, Mosby, 1996.
21. Khan F.M., *The Physics of Radiation Therapy, Second Edition*, Williams and Wilkins, 1994.
22. Johns H.E. and Cunningham J.R., *The Physics of Radiology, Fourth Edition*, Charles C Thomas Publisher, Illinois, 1983.
23. Curry T.S. et al. *Christensen's Introduction to the Physics of Diagnostic Radiology, Third Edition*, Lea and Febiger, Philadelphia, 1984.
24. Graham D.T., *Principles of Radiological Physics, Third Edition*, Churchill Livingstone, 1996.
25. Mckinlay A.F., *Thermoluminescence Dosimetry*, Adam Hilger Ltd, Great Britain, 1981.

26. Driscoll C.M.H, *Practical Aspects of Thermoluminescence Dosimetry-Conference Report Series 43*, Hospital Physics Association, 1984.
27. Dorthe M. and Cossmann P.H., *CT treatment planning based on a simulator-CT option: comparison between calculation and measurements using TLDs in a humanoid phantom*, Z. med. Phys., 12, 238-245, 2002.
28. The Hospital Physicists Association, *Phantom Materials for Photons and Electrons*, 1977, London.
29. Dunscombe P. et al, *Anthropomorphic phantom measurements for the validation of treatment planning system*, Phys. Med. Biol. 41, 399 – 411,1996.
30. Mayles W.P.M. et al, *Treatment verification and in vivo dosimetry*, Radiotherapy Physics in Practice, Oxford University Press, Oxford, 1993.
31. Venslaar J. et al, *Tolerances for the accuracy of photon beam dose calculation of treatment planning systems*, Radiotherapy and Oncology, 60, 191-201, 2001.
32. Low D. et al, *Phantoms for IMRT dose distribution measurements and treatment verification*, Int. J. Radiation Oncology Biol. Phys, 40, 1231-1235,1998.
33. ICRU Report 29, *Dose specification for reporting external beam therapy with photons and electrons*, Washington, USA, 1978.
34. Chen G.T.Y. and Pelizzari C.A., *The role of imaging in Tumor localization and portal design*, Radiation Therapy Physics, edited by Smith A.R., Springer, Berlin, 1995.
35. Galvin J.M., *The CT-simulator and the Simulator-C T: advantages, disadvantages and future developments*,
36. Coolens C and Childs P.J., *Calibration of CT Hounsfield units for radiotherapy treatment planning patients with metallic hip prosthese: the use of the extended CT-scale*, Physics in Medicine and Biology, 48,1591-1603,2003.
37. Quach K.Y. et al, *measurement of radiotherapy x-ray skin dose on a chest wall phantom*, Med. Phys. 27, 1676-1679.
38. Low D.A. et al, *Quantitative dosimetric verification of an IMRT planning and delivery system*, Radiotherapy and Oncology, 49, 305-316,1998.
39. Ahnesjö A. and Aspradakis M.M., *Dose for external photon beams in radiotherapy*, Physics in Medicine and Biology, 44, R99-155, 1999.

40. Meigooni A.S. et al, *Evaluation of the veridose QC phantom*, Medical Dosimetry, 28, 49-54, 2003.
41. Esthappan J. et al, *Dosimetry of therapeutic photon beams using an extended dose range film*, Medical Physics, 29, 2438-2445,2002.
42. Kirby T.H. et al, *Uncertainty analysis of absorbed dose calculations from thermoluminescence dosimeters*, Medical Physics, 19, 1427-1433, 1992.
43. Bucciollini M. et al, *Verification of IMRT fields by film dosimetry, Medical physics*, 31, 161-168, 2004.
44. Ju S.G. et al, *Film dosimetry for intensity modulated radiation therapy: Dosimetric evaluation*, Medical Physics, 29, 351-355,2002.
45. Mayer R. et al, *Two dimensional film dosimetry application in heterogeneous materials exposed to megavoltage photon beams*, Medical Physics, 24, 455-460, 1997.
46. Olch A.J., *Dosimetric performance of an enhanced dose range radiographic film for intensity –modulated radiation therapy quality assurance*, Medical Physics, 29, 2159-2168, 2002.
47. Stern R.L. et al, *Film dosimetry in the peripheral region using multiple sensitometric curves*, Medical Physics, 31, 327-332, 2004.
48. Arora V.R. and Weeks K.J., *Characterization of gypsum attenuators for radiotherapy dose modification*, Medical Physics, 21, 77-80,1994.
49. Glasgow G.P. et al, *Refined Gypsum effective attenuation coefficients for Co-60, 6MV, 10MV and 18MV x-rays*, Physics in Medicine and Biology, 48, 63-71, 2003.
50. Castellanos M.E. and Rosenwald J.C., *Evaluations of the scatter field for high-energy photon beam attenuators*, Physics in Medicine and Biology, 43, 277-290, 1998.